Stem Cell Reports
Article

ISSCR

OPEN ACCESS

miR-133a Enhances the Protective Capacity of Cardiac Progenitors Cells after Myocardial Infarction

Alberto Izarra,[1,2,9] Isabel Moscoso,[2,3,9] Elif Levent,[4] Susana Cañón,[1,2] Inmaculada Cerrada,[5,6] Antonio Díez-Juan,[2,5] Vanessa Blanca,[2] Iván-J. Núñez-Gil,[7] Iñigo Valiente,[2] Amparo Ruíz-Sauri,[8] Pilar Sepúlveda,[5] Malte Tiburcy,[4] Wolfram-H. Zimmermann,[4] and Antonio Bernad[1,2,*]

[1]Immunology and Oncology Department, National Center for Biotechnology, CSIC, 28049 Madrid, Spain
[2]Department of Cardiovascular Development and Repair, Fundación Centro Nacional de Investigaciones Cardiovasculares Carlos III, 28029 Madrid, Spain
[3]Cardiovascular Area, CIMUS, University of Santiago de Compostela-Instituto de Investigación Sanitaria, 15706 Santiago de Compostela, Spain
[4]Institute of Pharmacology, Heart Research Center Göttingen, University Medical Center, Georg-August University Göttingen and DZHK (German Center for Cardiovascular Research), 37075 Göttingen, Germany
[5]Instituto de Investigación Sanitaria INCLIVA, 46010 Valencia, Spain
[6]Unidad de Cardioregeneración, Hospital La Fe, 46009 Valencia, Spain
[7]Servicio de Cardiología, Hospital Clínico San Carlos, 28040 Madrid, Spain
[8]Departamento de Patología, Facultad de Medicina, Universidad de Valencia, 46010 Valencia, Spain
[9]Co-first author
*Correspondence: abernad@cnb.csic.es
http://dx.doi.org/10.1016/j.stemcr.2014.10.010

SUMMARY

miR-133a and miR-1 are known as muscle-specific microRNAs that are involved in cardiac development and pathophysiology. We have shown that both miR-1 and miR-133a are early and progressively upregulated during in vitro cardiac differentiation of adult cardiac progenitor cells (CPCs), but only miR-133a expression was enhanced under in vitro oxidative stress. miR-1 was demonstrated to favor differentiation of CPCs, whereas miR-133a overexpression protected CPCs against cell death, targeting, among others, the proapoptotic genes *Bim* and *Bmf*. miR-133a-CPCs clearly improved cardiac function in a rat myocardial infarction model by reducing fibrosis and hypertrophy and increasing vascularization and cardiomyocyte proliferation. The beneficial effects of miR-133a-CPCs seem to correlate with the upregulated expression of several relevant paracrine factors and the plausible cooperative secretion of miR-133a via exosomal transport. Finally, an in vitro heart muscle model confirmed the antiapoptotic effects of miR-133a-CPCs, favoring the structuration and contractile functionality of the artificial tissue.

INTRODUCTION

Cardiovascular diseases are the major cause of illness and death in developed countries, and transplantation of progenitor cells has emerged as a bona fide therapeutic option for this group of diseases. Currently, cell therapy approaches with diverse types of mature or stem cell populations have produced modest improvements (Sanganalmath and Bolli, 2013). Among them, resident cardiac stem/progenitor cells (CSCs/CPCs) are a promising option (Chugh et al., 2012, Malliaras et al., 2014). Many experimental adult CPC populations have been isolated, based on a specific surface marker profile or their differentiation potential. The most studied are c-KIT$^+$, SCA-1$^+$, cardiosphere-derived cells, and cardiac mesoangioblasts, all of which have demonstrated regenerative potential in vivo (Beltrami et al., 2003, Galvez et al., 2008, Malliaras et al., 2012, Oh et al., 2003, Tateishi et al., 2007). However, transplanted cells die in large numbers in the infarcted myocardium shortly after transplantation, presenting a hurdle to improving heart function through stem cell therapy (Robey et al., 2008). The infarct microenvironment is characterized by hypoxia, oxidative stress, and proapoptotic and inflammatory factors (Hori and Nishida, 2009); thus, a deeper understanding of how transplanted progenitor cells engraft and survive in this hostile context is required to enhance their clinical usefulness.

microRNAs (miRNAs) are small noncoding RNAs of 22 nucleotides that control gene expression chiefly by translational repression (Lee et al., 2004). miRNA expression is spatially and temporally regulated during development, and they can participate in the regulation of pluripotent stem cell lineage commitment (Ivey et al., 2008). miR-1 and miR-133a belong to the MyomiR group of muscle-specific miRNAs. They regulate heart and skeletal muscle biology and play an important role in heart development (Liu et al., 2008, Matkovich et al., 2010). Both miRNAs are transcribed from the same locus and are processed as a bicistronic transcript. This locus is duplicated in the genome, although mature miRNA forms are identical from both loci (Townley-Tilson et al., 2010). Their expression is controlled by serum response factor (SRF), MEF2, and MyoD transcription factors, which bind to sequences located upstream from the miRNAs and/or to their intergenic sequences (Liu et al., 2008, Zhao et al., 2005). Overexpression of miR-1 mediates cardiomyocyte withdrawal

from the cell cycle through the targeting of *Hand2*. Conversely, mice deficient for miR-1-2 have an elevated number of postnatal cardiomyocytes proliferating and present an enlargement of ventricular walls (Zhao et al., 2007). Double knockout mice for both mature forms of miR-133a exhibit excessive cardiomyocyte proliferation and increased apoptosis associated with an elevated expression of their targets SRF and cyclin D2, leading to ventricular-septal defects (Zhao et al., 2007). However, overexpression of miR-133a in postnatal cardiomyocytes (Matkovich et al., 2010) or under the control of a muscle-specific promoter (Deng et al., 2011) has no significant effect.

miR-1 and miR-133a have been implicated in pathological processes such as hypertrophy (Liu et al., 2008, Matkovich et al., 2010, Zhao et al., 2005, 2007), and their levels may define a predisease stage. A recent meta-analysis (comprising 15 studies and 2,136 patients) demonstrated the validity of miR-133a and miR-499 levels in plasma or serum as a diagnostic biomarker of myocardial infarction (MI) (Cheng et al., 2014). However, analysis of surgical samples of the right atrial myocardium of patients showed that miR-133 expression decreased significantly as the severity of heart failure increased; no correlation was found for miR-1 (Danowski et al., 2013). Furthermore, miR-133a is downregulated in response to transaortic constriction-induced hypertrophy and after MI in mice, rats, pigs, and humans (Carè et al., 2007, Hullinger et al., 2012, He et al., 2011) and also in diabetic cardiomyopathy (Chen et al., 2014, Yildirim et al., 2013). Downregulation of miR-133a has been also associated with several vascular pathologies such as atherosclerosis, intracranial aneurysms, and arterial calcification (Gao et al., 2014, Jiang et al., 2013, Liao et al., 2013).

miR-1 and miR-133a have been demonstrated to influence embryonic stem (ES) cell fate; in fact, overexpression of each miR in mouse and human ES cells promotes mesoderm specification while suppressing other lineages (Ivey et al., 2008). Ivey and Srivastava (2010) showed that forced miR-1 expression alone was sufficient to drive expression of cardiogenic markers, while miR-133a overexpression blocked this process. Controversially, other studies have described that miR-1 overexpression reduces the expression of cardiac markers in mouse ES cells (Takaya et al., 2009). Therefore, thorough knowledge about how miR-1 and miR-133a influence cardiac differentiation of pluripotent and multipotent cells is needed. In addition, apart from their central role in heart function, they are also implicated in a regulatory network of miRNAs controlling osteoblastic and chondrogenic differentiation of MSCs (Li et al., 2008, Wang et al., 2012). Collectively, these examples illustrate the putative central role of these muscle-specific miRNAs in cellular homeostasis.

In this work, we describe a role for miR-133a in the survival regulation of a Sca-1$^+$ CPC population, which shares features with other populations of mesenchymal stem cells (MSCs) in terms of surface marker profile and differentiation potential. Interestingly, miR-133a promotes survival of CPCs under oxidative stress by decreasing caspase 3 activity and targeting the proapoptotic genes *Bim* and *Bmf*. Furthermore, transplantation of miR-133a-CPCs significantly improves heart function in murine models of acute MI by reducing cardiac hypertrophy and cardiomyocyte apoptosis and increasing *bFgf*, *Vegf*, *Igf1*, and *Hgf* expression in vitro. Finally, we describe that the majority of secreted miR-133a is localized in the exosomal fraction of miR-133-CPCs.

RESULTS

Role of miR-1 and miR-133a in Adult CPCs

CPCs from adult mouse hearts accounted for 7%–20% of the myocyte-depleted small cells from the myocardium (Figures S1A and S1B available online) and endowed cardiac, endothelial, and smooth-muscle differentiation capacity (Figures S1C and S2). In addition, mouse CPCs also demonstrated MSC-like differential potential (Figures S1D and S1E) as previously shown for human counterparts (Moscoso et al., 2013). miR-1 and miR-133a expression was under the detection level in undifferentiated CPCs, but exposure to cardiac differentiation conditions (Figure 1A) or coculture with neonatal rat cardiomyocytes (NRCMs; Figure 1B) progressively increased the expression of miR-1 and miR-133a.

To analyze the influence of both myomiRs in CPCs differentiation capacity, we transduced them with retroviral vectors encoding miR-1, miR-133a, or a control miRNA (Figure S3A). After dexamethasone (Dex) induction, we analyzed *Nkx2.5* and *Troponin T* expression as early and late cardiac markers, respectively. Interestingly, whereas miR-1-CPCs showed a significant increase in *Nkx2.5* expression, both in basal conditions and after cardiac induction with Dex, miR-133a-CPCs did not display any significant modification (Figure S3B). Evaluation of levels of *Troponin T*, after induction (Dex), rendered a similar result (Figure S3C). This strongly suggests that forced expression of miR-1 could be favoring cardiac commitment and differentiation of CPCs, whereas overexpression of miR-133a does not seem to modulate significantly these processes. Neither of the transduced miRNAs affected the proliferation, as measured by 3-(4,5-dimethylthiazol-2-yl)-2,5-diphenyltetrazolium bromide (MTT) assay or ^{3}H-thymidine incorporation (Figures S3D and S3E) or apoptosis rates (data not shown) of CPCs, in basal conditions.

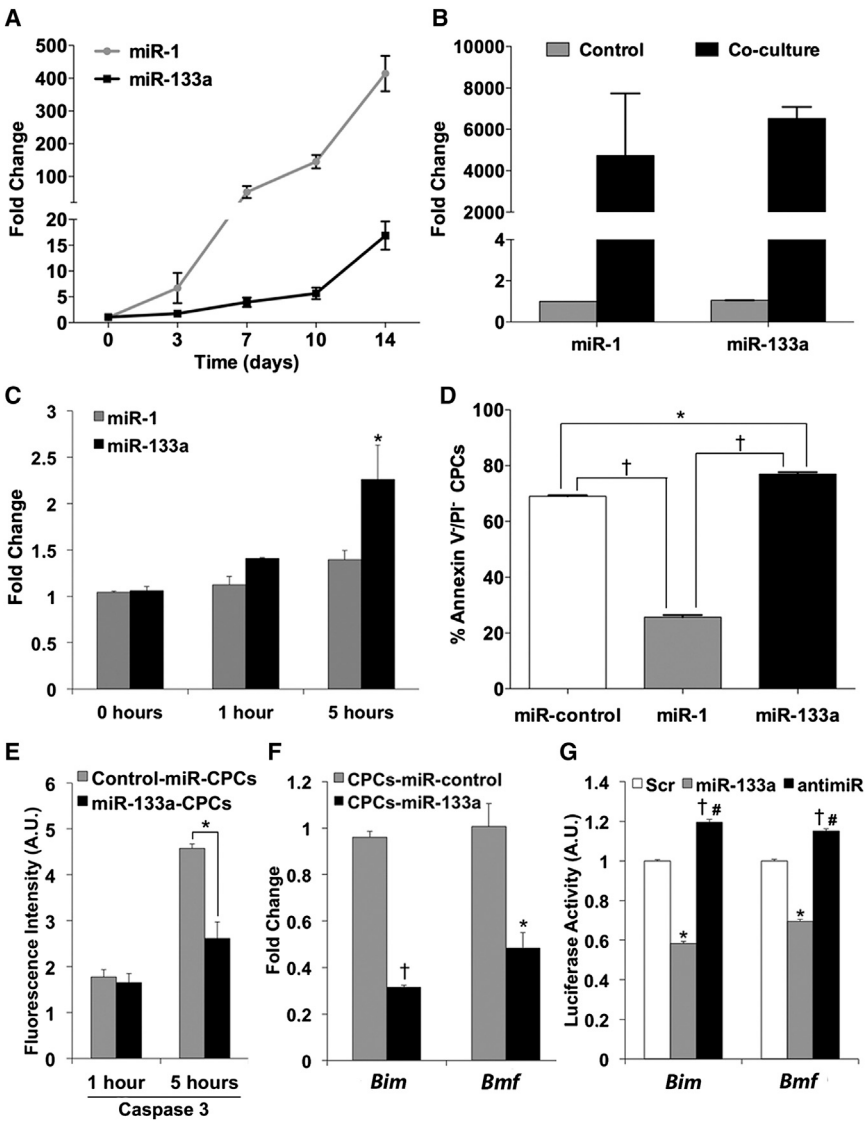

Figure 1. Role of miR-1 and miR-133a in CPC Differentiation and Response to Oxidative Stress

(A) Quantitative RT-PCR analysis of miR-1 and miR-133a expression in CPCs exposed to cardiac differentiation medium.

(B) miR-1 and miR-133a expression in CPCs after 7 day co-culture with NRCMs.

(C) miR-1 and miR-133a expression in CPCs after treatment with H_2O_2 (n = 3, *p < 0.05 versus miR-133a at 0 hr).

(D) Fluorescence-activated cell sorting (FACS) analysis of live CPCs (annexin V−/PI− cells) after 5 hr of H_2O_2 treatment (n = 3; †p < 0.01, *p < 0.05).

(E) Caspase 3 activity measured by FACS (mean fluorescence intensity) 1 and 5 hr after H_2O_2 treatment (n = 3; *p < 0.005).

(F) Gene expression analysis of *Bim* and *Bmf* after H_2O_2 treatment (5 hr; n = 3; †p < 0.00005, *p < 0.005).

(G) 3′UTR reporter assay for *Bim* and *Bmf*. *Renilla* luciferase activity was assayed 24 hr after transfection, and the values were normalized to the activity of firefly luciferase encoded in the same vector (n = 3; *Bim*: *p < 0.00005, †p < 0.001 versus Scr, #p < 0.00005 versus miR-133a; *Bmf*: *p < 0.0001, †p < 0.001 versus Scr, #p < 0.00005 versus miR-133a).

(C–G) Data are mean ± SEM, n = 3 experiments. See also Figures S3 and S4.

In an in vitro model of induced oxidative stress injury, only miR-133a was significantly upregulated upon treatment of CPCs with H_2O_2 (200 μM; 1–5 hr) (Figure 1C). Importantly, miR-1-CPCs displayed increased apoptosis in comparison with both control-miR-CPCs and miR-133a-CPCs (Figures 1D, S4A, and S4B). A significant increase in caspase 3 activity in control cells was prevented in miR-133a-CPCs (Figure 1E); a comparable result was obtained by measurement of cytosolic cytochrome c (Figure S4C).

Bioinformatic Prediction of miR-133a Targets

Bioinformatic analysis of putative target genes for miR-133a by Ingenuity Pathway Analysis software predicted cell death as the main biological function affected at organ and cellular level and hypertrophy, fibrosis, and apoptosis as the main toxic processes altered. We found common targets as *Bmf* (*Bcl-2* modifying factor) and *Bim* (*Bcl2l11*), which are potent proapoptotic factors (reviewed by Piñon et al., 2008), a serine threonine kinase *Stk4* (formerly *Mst1*) activated by oxidative stress (Cottini et al., 2014, Del Re et al., 2014), and finally *Foxo1* that has been described as a critical promotor of cardiomyocyte survival upon oxidative stress conditions (Puthanveetil et al., 2013). Particularly interesting is the recent implication of *Bmf* in oxidative stress-induced apoptosis of hepatic progenitor populations after activation of transforming growth factor β (TGF-β) signaling (Martínez-Palacián et al., 2013), which was predicted in our analysis as putative upstream regulator of *Bmf*, *Bim*, and *Foxo1* (see Supplemental Experimental Procedures; Figures S5 and S6A).

Quantitative RT-PCR (RT-qPCR) analysis of miR-133a-CPCs versus miR-control-CPCs, challenged with H_2O_2,

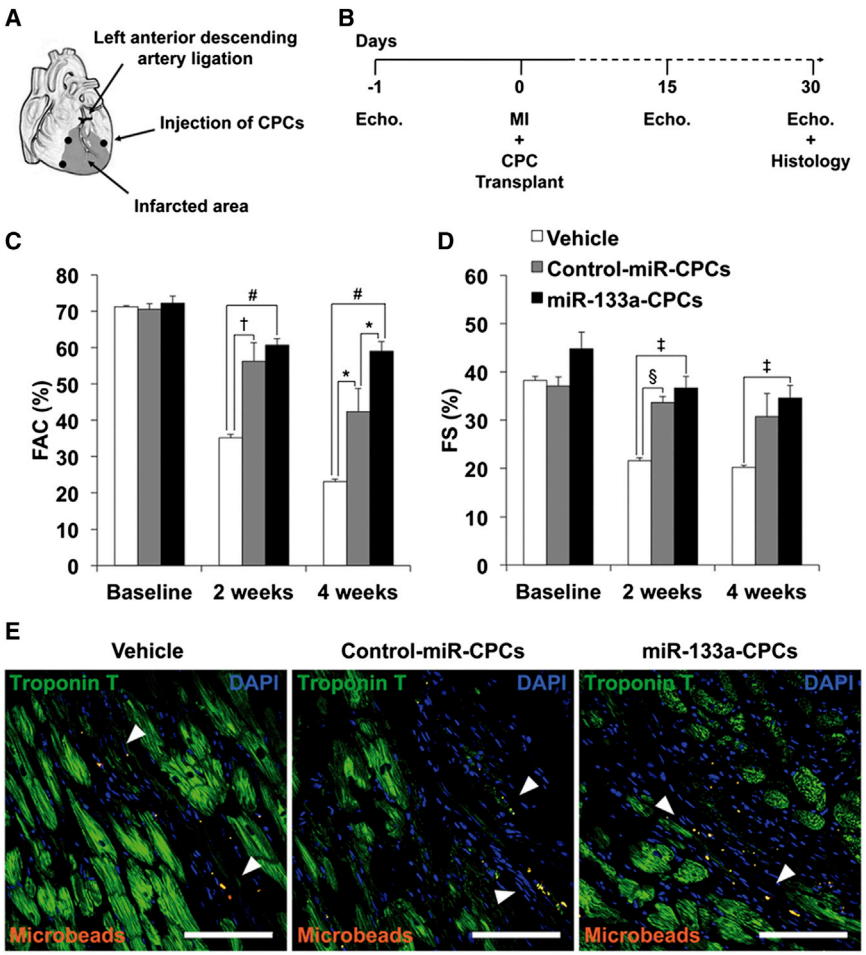

Figure 2. CPC Transplantation in a Rat Model of MI

(A) Diagram of in vivo transplantation of CPCs. After ligation of the left descending coronary artery, vehicle, control-miR-CPCs or miR-133a-CPCs were injected together with red fluorescent microbeads as a marker for injected material, into three locations at the infarct border.

(B) Experimental timeline of echocardiography analysis.

(C and D) Echocardiography measurements of FAC (C) and FS (D) (hearts: vehicle n = 5; control-miR–CPCs n = 6; miR-133a–CPCs n = 11. *$p < 0.05$, †$p < 0.01$, ‡$p < 0.005$, §$p < 0.0005$, #$p < 0.000005$).

(E) Detection of fluorescent microbeads (white arrowheads) in the infarct border zone (white bars are 100 μm). Data are mean ± SEM. See also Table S3.

showed that although the expression of all these predicted targets was effectively downregulated, *Bim* and *Bmf* were specially affected (Figures 1F and S6B). To confirm whether miR-133a could modulate directly the expression of *Bim* and *Bmf*, we cloned separately a 1kb fragment of their 3′UTRs containing predicted binding sites for miR-133a, downstream of the *Renilla* luciferase reporter and transfected 293T cells with the constructs. The cotransfection with a synthetic precursor of miR-133a significantly reduced luciferase activity in both cases with respect to a scramble miRNA, while cotransfection with a miR-133a inhibitor abolished this reduction (Figure 1G).

miR-133a-CPCs Protect Cardiac Function

To evaluate the potential protective effect of miR-133a in vivo, GFP-tagged CPCs (10^5) expressing control miRNA or miR-133a were injected into the infarct border zone in a MI model in immunosuppressed rats (Figure 2A). Cardiac function was monitored by echocardiography 1 day before MI and 2 and 4 weeks after MI and CPC/vehicle injection (Figure 2B). Compared with vehicle injection, animals injected with CPCs showed significantly greater fractional area change (FAC) at 2 weeks after MI, but no significant differences were observed between rats injected with control-miR-CPCs and miR-133a-CPCs. However, at 4 weeks after MI, animals injected with miR-133a-CPCs showed significantly greater FAC compared with animals injected with either vehicle or control-miR-CPCs (Figure 2C; Table S3). Similarly, fractional shortening (FS) at 2 weeks after MI was increased by injection with CPCs, independently of miRNA expression, but at 4 weeks after MI, this increase was sustained only in rats injected with miR-133a-CPCs (Figure 2D; Table S3). No GFP^+ cells could be found on heart sections 4 weeks after transplant (Figure 2E); similar results were obtained using a syngeneic mouse MI model, in which GFP^+ CPCs could be detected at low numbers within the first postinjection days, although a clear advantage for miR-133a-CPCs was not evidenced (unpublished data).

Morphometric analysis of explanted hearts 4 weeks after MI showed severe left ventricle chamber dilatation and infarct wall thinning in vehicle-treated animals

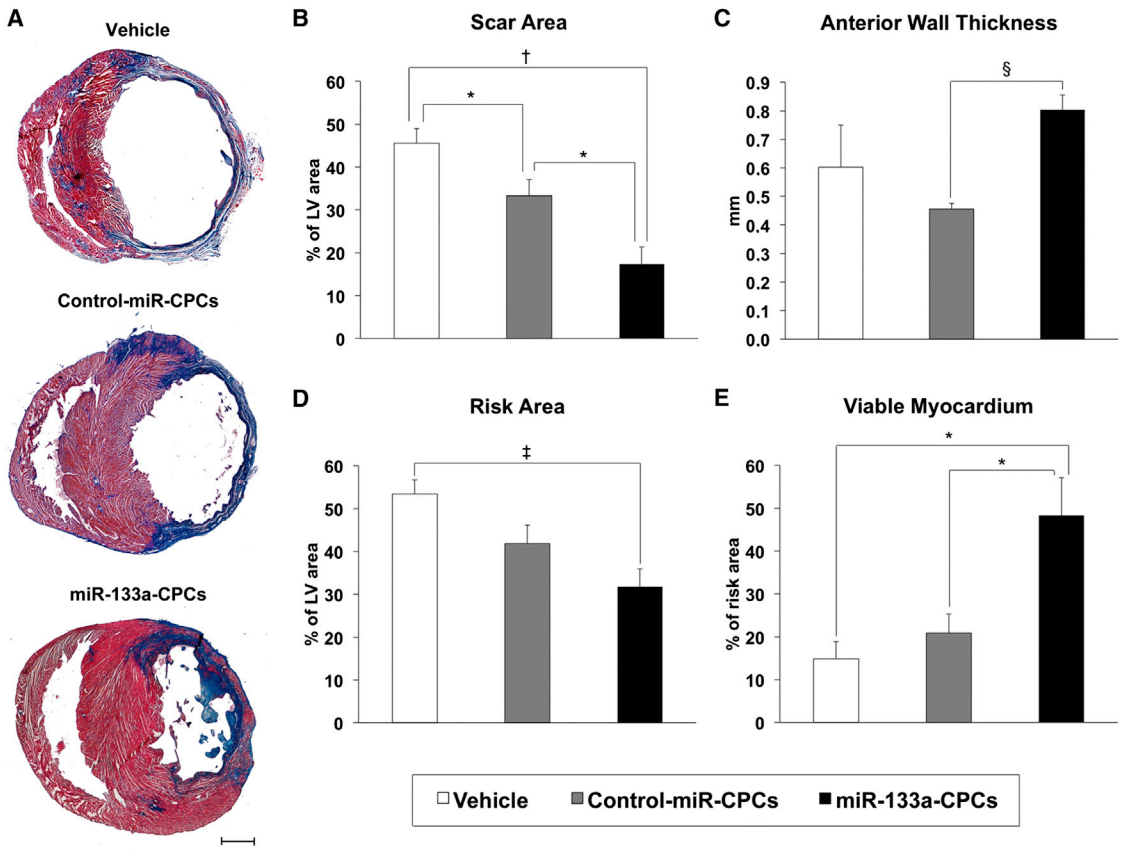

Figure 3. Morphometric Analysis

(A) Representative Masson's trichrome-stained myocardial sections of infarcted rat hearts 4 weeks after injection with vehicle, control-miR-CPCs, or miR-133a-CPCs. Scar tissue and viable myocardium are identified as blue and red, respectively (the scale bar represents 2 mm). (B–E) Left ventricle morphometric parameters. (B) Scar area. (C) Anterior wall thickness. (D) Risk area and (E) viable myocardium inside the risk area (hearts: vehicle n = 5; control-miR-CPCs n = 7; miR-133a-CPCs n = 7. *$p < 0.05$, †$p < 0.005$, ‡$p < 0.001$, §$p < 0.00005$). Data are mean ± SEM. See also Table S4.

(Figure 3A; Table S4). Transplantation of control-miR-CPCs significantly decreased the scar area with respect to vehicle-treated animals, although no significant differences were found in infarcted wall thickness or viable myocardium inside the risk area (Figures 3B–3E). However, transplantation with miR-133a-CPCs further decreased the scar area and infarcted wall thinning compared with vehicle and control-miR-CPCs (Figures 3B and 3C). While the risk area decreased with respect to vehicle-treated animals, with no significant differences between the two CPC-injected groups (Figure 3D), the amount of viable myocardium inside the risk area (Figure 3E) was significantly higher in hearts injected with miR-133a-CPCs.

CPCs Increase Vascularization and Protect against Hypertrophy

Hearts from animals treated with control-miR-CPCs or miR-133a-CPCs contained a higher density of α-smooth muscle actin $(\alpha\text{-SMA})^+$ blood vessels in the infarct border zone compared with vehicle-treated animals (Figure 4B), but there were not significant differences in the remote zone (Figure 4A). Nonetheless, the density of $\alpha\text{-SMA}^+$ blood vessels in the border zone did not differ between hearts injected with control-miR-CPCs or miR-133a-CPCs (Figure 4D). We also investigated the capacity of CPCs to promote new cardiomyocyte formation (Figure 4C). Even though CPC injection did not significantly increase the total number of EdU^+ nuclei, both control-miR-CPCs and miR-133a-CPCs significantly increased the percentage of DNA-replicating cardiomyocytes (EdU^+/troponin T^+ cells) 4 weeks after MI, although this increase was smaller for animals injected with miR-133a-CPCs (Figure 4E).

We also measured the extent of hypertrophy in the border zone of infarcted rat hearts (Figure 5A). Cardiomyocyte cross-sectional area was significantly lower in animals injected with control-miR-CPCs compared with

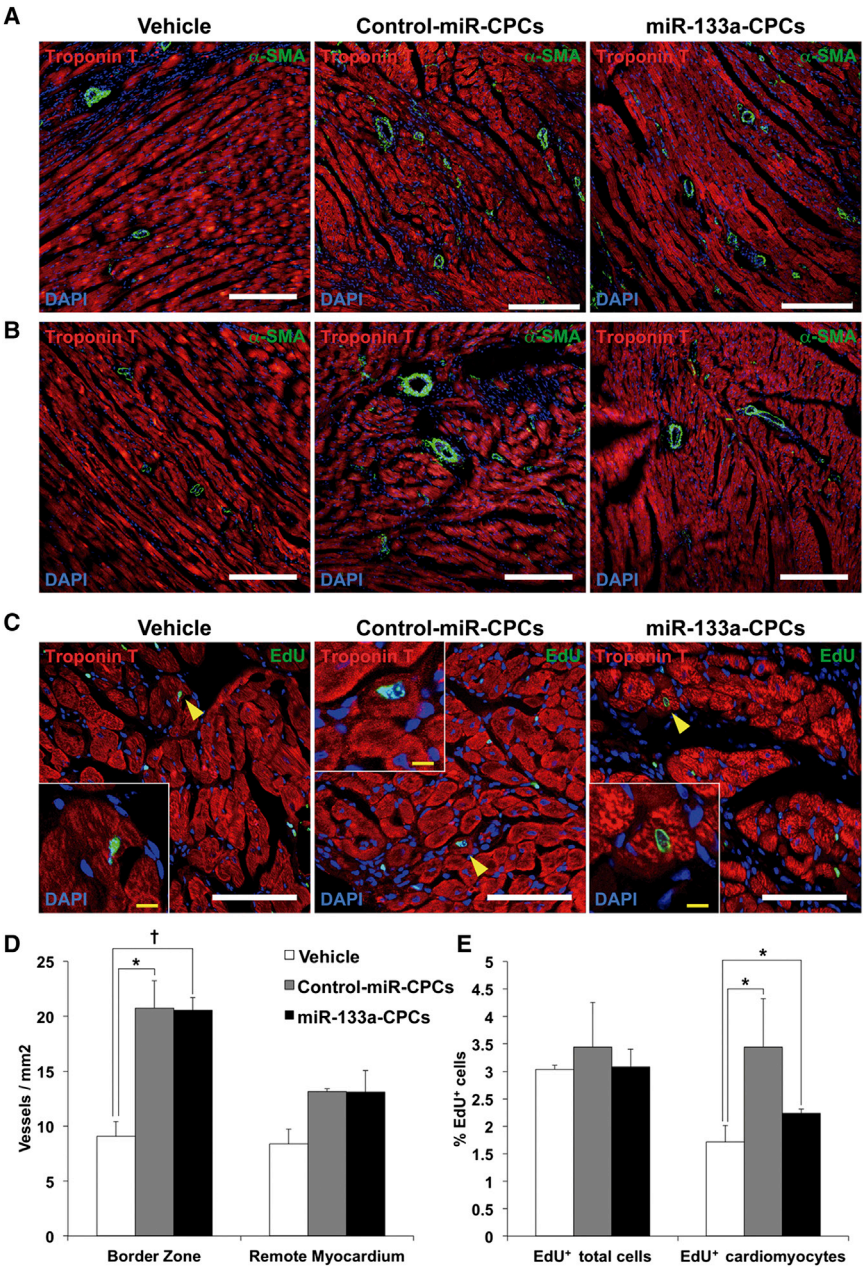

Figure 4. Effect of CPC Transplantation on Vascular Density and Cardiomyocyte Proliferation

(A and B) Representative immunofluorescence on rat heart sections taken from the infarction zone (A) and the healthy myocardium (B) 4 weeks after MI and injection with vehicle, control-miR-CPCs, or miR-133a-CPCs. Sections were stained for α-SMA and troponin T to reveal the density of α-SMA+ blood vessels (white bars are 200 μm).

(C) Representative sections from border zone, stained for EdU and troponin T (yellow arrowheads indicate EdU+/troponin T+ cardiomyocytes; white bars indicate 100 μm, and yellow bars show 10 μm).

(D) Quantification of α-SMA+ blood vessels/mm^2 (hearts: vehicle n = 3; control-miR–CPCs n = 3; miR-133a-CPCs, n = 4, *p < 0.05, †p < 0.005).

(E) Quantification of EdU+ total cells and EdU+/troponin T+ cardiomyocytes (hearts: vehicle n = 3; control-miR-CPCs n = 3; miR-133a-CPCs, n = 3, *p < 0.05).

Data are mean ± SEM.

vehicle-injected animals (Figure 5B), and this reduction was higher with miR-133a-CPCs. Pathological hypertrophy is linked to the activation of a fetal cardiac gene program (Liu et al., 2008). An assessment of key fetal and adult cardiac genes expression revealed that animals treated with miR-133a-CPCs showed a significant reduction in the expression ratios of *β-Mhc/α-Mhc* and, more pronouncedly, in the *ANP/BNP* ratio (Figure 5C) when compared with animals treated with control-miR-CPCs, suggesting that miR-133a-CPCs protected the heart from pathological hypertrophy.

We tested conditioned medium (CM) from CPCs in an in vitro model of angiotensin II (ANG II)-induced hypertrophy in NRCMs (Figures 5D and 5E). ANG II-stimulated NRCMs cultured in control medium are larger than nonstimulated cells (Figure 5D). In contrast, culture of NRCMs in CM from miR-133a-CPCs exhibited a significant decrease in ANGII-induced hypertrophy, and cardiomyocyte area was comparable to nonstimulated cells (Figure 5E). All together, these results suggested that miR-133-CPC transplantation would improve cardiac function mainly by protecting resident cardiomyocytes

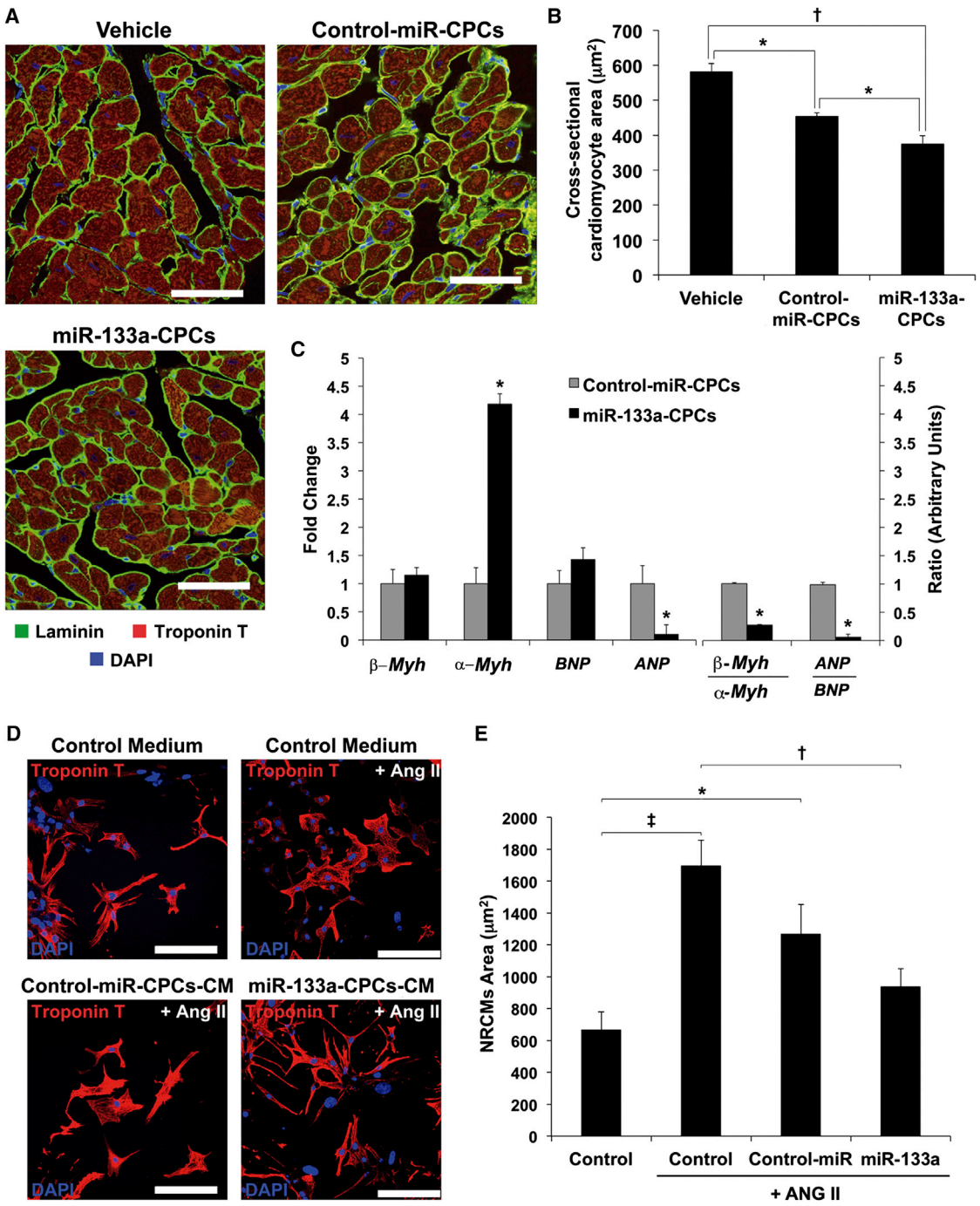

Figure 5. Effect of miR-133a-CPCs on Cardiac Hypertrophy Parameters

(A) Representative immunofluorescence on rat heart sections taken from the infarct border zone 4 weeks after injection with vehicle, control-miR-CPCs, or miR-133a-CPCs. Sections were stained for laminin and troponin T in order to determine cardiomyocyte cross-sectional area (scale bars represent 50 μm).

(B) Quantification of cardiomyocyte cross-sectional (hearts: vehicle n = 3; control-miR-CPCs n = 8; miR-133a-CPCs, n = 8, *$p < 0.05$, †$p < 0.001$).

(C) RT-qPCR analysis of fetal and adult cardiac genes at 4 weeks after MI (hearts: control-miR-CPCs, n = 8, miR-133a-CPCs, n = 6; *$p < 0.05$).

(D and E) Effect of CPC-CM on ANGII-induced hypertrophy in NRCMs in vitro. (D) Representative troponin T staining in the presence of control medium, control-miR-CPC-CM or miR-133a-CPC-CM (bars, 100 μm). (E) Quantification of cardiomyocyte area (n = 3 experiments; *$p < 0.05$, †$p < 0.01$, ‡$p < 0.005$).

Data are mean ± SEM.

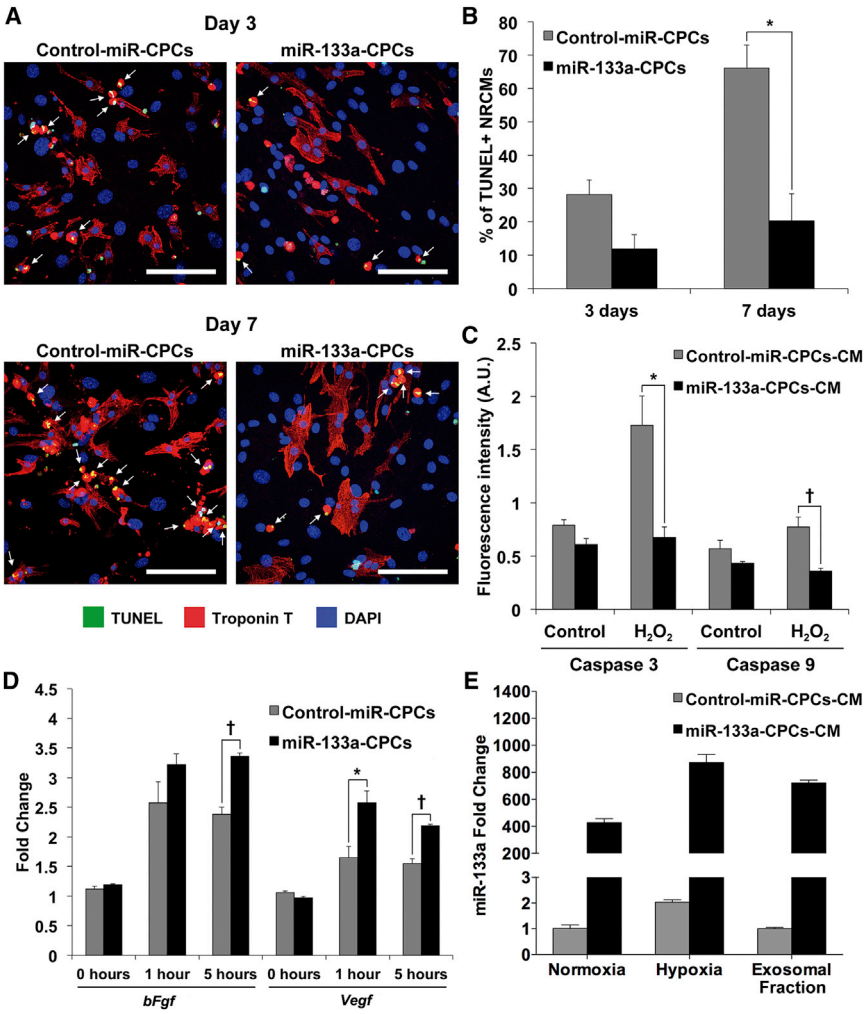

Figure 6. Effect of miR-133a-CPCs on Cardiomyocyte Apoptosis

(A) Representative immunofluorescence images of NRCMs cocultured with control-miR-CPCs or miR-133a-CPCs and serum starved for 3 or 7 days. Apoptosis was detected by TUNEL assay (yellow spots indicated by white arrows). Troponin T, red; DAPI-stained nuclei, blue; scale bars represent 100 μm).

(B) Quantification of apoptotic cardiomyocytes (TUNEL+/troponin T+ cells) after 3 and 7 days of serum starvation (n = 3 experiments; *p < 0.05).

(C) Effect of CPC-CM on H_2O_2-induced cardiomyocyte apoptosis (caspase 3/caspase 9 activity; n = 3 experiments, two replicates per experiment; *p < 0.01, †p < 0.005).

(D) RT-qPCR analysis of *bFgf* and *Vegf* during H_2O_2-induced apoptosis in CPCs (1–5 hr, n = 3 experiments, *p < 0.05, †p < 0.005).

(E) RT-qPCR analysis of miR-133a in CPC-CM after 48 hr in normoxia (20% O_2) and hypoxia (1% O_2) and in the purified exosomal fraction (normoxia), n = 3 experiments. Data are mean ± SEM.

from stress conditions rather than inducing regeneration of the endogenous damaged population, which is consistent with other reports using cell therapy approaches (Wang et al., 2009).

To test this hypothesis, we cocultured control-miR-CPCs and miR-133a-CPCs with NRCMs in serum-free medium to mimic stress conditions. Analysis of double-stained TUNEL$^+$/troponin T$^+$ cardiomyocytes revealed that coculture with miR-133a-CPCs significantly and specifically reduced (>40%) the number of apoptotic NRCMs after 7 days (Figures 6A and 6B). In order to determine whether this effect required direct cell-to-cell interaction, we cultured NRCMs overnight with CM from control-miR-CPCs or miR-133a-CPCs, followed by exposure to H_2O_2 (200 μM) for 2 hr. CM from miR-133a-CPCs significantly reduced activation of caspases 3 and 9 (Figure 6C). Growth factor expression analysis showed that *Vegf* and *bFgf* levels, after H_2O_2 treatment for 1 and 5 hr, were significantly increased in miR-133-CPCs (Figure 6D), suggesting that higher release of these cytokines could mediate their protective effects via paracrine actions.

Recent studies have solidly established exosomes as paracrine effectors transferring functional molecules between cells in many physiological and pathological processes (Bang et al., 2014). In human CPCs (hCPCs), a critical role for exosomes has been associated to their capacity for improving cardiac function after injury (Barile et al., 2014, Ibrahim et al., 2014). Based on these evidences, we analyzed the levels of miR-133a present in the CM (48 hr) from miR-133a-CPCs and control-miR-CPCs cultures, in basal conditions (normoxia) and after hypoxia (Figure 6E), which simulates the situation after MI. CM from miR-133a-CPCs contained very high amounts of miR-133a compared with those detected in CM from control-miR-CPCs. The differences were comparable to those found in the cellular fraction (Figure S3A). Furthermore, hypoxia (1% O_2) induced the increase of miR-133a levels secreted to the medium by 2-fold in both CPC populations. The analysis of purified exosomal fraction revealed that exosomes

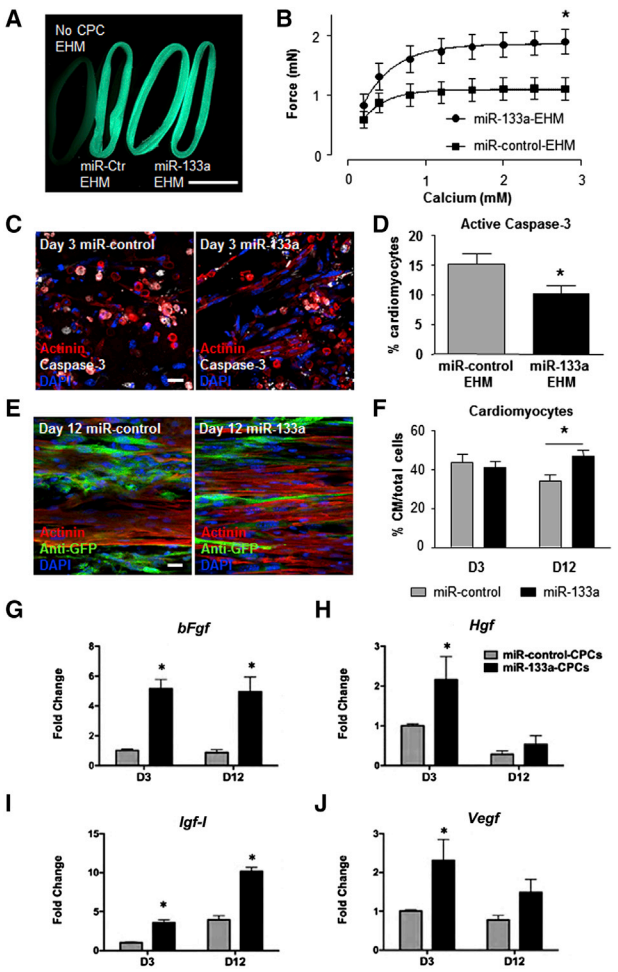

Figure 7. miR-133a-CPCs Enhance the Functionality of EHM

(A) GFP fluorescence on day 12 of culture of EHM with GFP-labeled miR-control-CPCs and miR-133a-CPCs compared with EHM without CPCs (left). The scale bar represents 5 mm.

(B) Calcium-induced contractile force of miR-control- or miR-133a-CPC EHM, n = 6 experiments, *p < 0.05.

(C) Representative staining of day 3 EHM cocultures with miR-control-CPCs (left) and miR-133a-CPCs (right) (actinin-α1, red; activated caspase 3, white; DAPI-stained nuclei, blue; scale bar represents 20 μm).

(D) Quantification of caspase 3-positive cardiomyocytes on day 3 of miR-control and miR-133a-CPCs-EHM cocultures; n > 1,000 cells from three experiments.

(E) Representative staining of cardiomyocytes and GFP$^+$-CPCs on day 12 of cocultured EHM (actinin-α1, red; anti-GFP, green; DAPI-stained nuclei, blue; scale bar represents 20 μm).

(F) Quantification of cardiomyocyte percentage on days 3 and 12 of miR-control-CPCs and miR-133a-CPC-EHM cocultures, n > 1,000 cells/group from two experiments (day 3) and three experiments (day 12, *p < 0.05).

(G–J) Expression of *bFgf, Hgf, Igf-1 and Vegf* in miR-control-CPCs (gray bars) and miR-133a-CPCs (black bars) in EHM cocultures at day 3 and day 12 (n = 3 experiments per group, *p < 0.05).

Data are mean ± SEM. See also Figure S7.

derived from control-miR-CPCs and miR-133a-CPCs were highly enriched in miR-133a, in relation to the whole CM.

Simulation of miR-133a-CPCs Protection in Engineered Heart Muscle

To investigate the responsiveness of heart muscle to miR-133a-CPCs in a controllable fashion, we used an in vitro heart muscle model, termed engineered heart muscle (EHM) (Tiburcy et al., 2011, Zimmermann et al., 2000, 2002). We generated cocultures of CPCs-EHMs by adding CPCs to isolated primary rat cardiomyocytes (84% ± 3% actinin-α1-positive, n = 4) in a 1:3 ratio (Figure 7A). In comparison with miR-control-EHM (containing control-miR-CPCs), the contractile force of miR-133a-EHM (containing miR-133a-CPCs) was significantly enhanced after addition of calcium to evoke contraction (Figure 7B). Given the demonstrated extensive cardiomyocyte death occurring during the first 3 days of EHM cultures (Tiburcy et al., 2011), we hypothesized that miR-133a-CPCs could protect cardiomyocytes against apoptosis in this period, leading to an increased number of viable cardiomyocytes at day 12 of culture. Indeed, we confirmed that caspase 3 activation, at day 3 of EHM culture, was reduced in miR-133a-EHM (Figures 7C and 7D). Consequently, we detected a higher percentage of cardiomyocytes in miR-133a EHM at day 12 when compared with miR-control cultures (Figures 7E and 7F). To clarify the nature of the support provided by miR-133a-CPCs to tissue formation, we analyzed the expression of growth factors. *Fgf*, *Hgf*, *Igf-1*, and *Vegf* levels were all increased in miR-133a-EHMs (Figures 7G–7J). Specially in early culture stages, we did not find a relevant modulation of additional prosurvival factors for cardiomyocytes as *Sdf-1*, a critical factor for the in vivo regeneration capacity of cardiospheres-derived cells (CDCs) (Malliaras et al., 2014) or *Sirt-1*, which protects the heart against oxidative stress when upregulated at moderate levels (Alcendor et al., 2007), but we found a clear upregulation of *S100a4* throughout the whole culture (Figure S7). *S100a4* has been shown to inhibit apoptosis and increase the survival capacity of cardiomyocytes after injury (Schneider et al., 2007). Accordingly, we found a highly significant difference (in early stages) in *Bmf* expression and a small not-significant difference in levels of *Bcl-2*, *Bcl-xl*, and *Bim*, suggesting that while *Bim* would be only relevant in CPCs, *Bmf* might mediate the protective role of miR-133 against stress-induced apoptosis, both in CPCs and cardiomyocytes.

DISCUSSION

Cardiac differentiation of Sca-1$^+$ CPCs is associated with a progressive increase in the expression of miR-1 and

miR-133a. Although overexpression of these miRNAs had little influence on proliferation or apoptosis of CPCs in basal conditions, miR-1 increased the level of apoptosis promoted by H_2O_2, while miR-133 increased the number of viable cells under the same conditions. This is consistent with prior findings demonstrating that expression of miR-1 is induced after exposure to H_2O_2, in both a dose- and time-dependent manner and that several cell types overexpressing miR-1 are more vulnerable to H_2O_2-induced oxidative stress (Chen et al., 2012). The antiapoptotic action of miR-133a has not been reported previously in stem cells or CSCs/CPCs. In cardiomyocytes, although the role of miR-133a during in vitro apoptosis has been questioned, it has been validated in in vivo studies (Liu et al., 2008, Matkovich et al., 2010). Some reports have recently suggested that caspase 9 might be a direct target of miR-133a since in vivo infusion of this miRNA after MI reduces caspase 9 activity and decreases the number of apoptotic cardiomyocytes (He et al., 2011).

Bioinformatic analysis of putative miR-133 target genes rendered candidates mainly related to cell death and heart damage events such as hypertrophy, fibrosis, and apoptosis. Among them, *Bim*, *Bmf*, *Stk4*, *and Foxo1* were involved in many of these processes. RT-qPCR analysis of miR-133a-CPCs versus miR-control-CPCs, treated with H_2O_2, demonstrated the potent proapoptotic factors *Bim* and *Bmf* were the most significantly downregulated. Among all BH3-only proteins known to date, *Bim* is the best described concerning its biological function, whereas little is known about its closest relative *Bmf*, which seems to play a more restricted role by supporting *Bim* in some cell death processes (Piñon et al., 2008). Recently, it was demonstrated that in mouse and human hematopoietic stem and progenitor cells, low expression of *Bim* or *Bmf* provokes a similar effect to overexpression of *Bcl-2* and that their downregulation inhibits apoptosis, favoring HSC long-term engraftment (Labi et al., 2013). Furthermore, *Bim* is an important target for a miRNA cocktail (miR-21, miR-24, and miR-221) that significantly improves survival of untreated $Sca1^+$CPCs (Hu et al., 2011). In agreement with these data, our results suggest that miR-133 protects CPCs from oxidative stress-induced apoptosis, at least in part, through targeting of *Bmf* and *Bim*. In addition, we found an increase of expression of *bFgf* and *Vegf* in miR-133-CPCs after treatment with H_2O_2 and a clear downregulation of caspase 3 and *Bmf* what would support the antioxidative role in miR-133 in CPCs.

GFP^+ CPCs or GFP^+ CPC-derived cells were not detected in rats 4 weeks after injection in infarcted hearts. This result is consistent with other previous studies where no or very few cells were found 1 month after cell administration. Overall, this implies that direct differentiation of implanted cells is not responsible for the improved cardiac function; accordingly, paracrine stimulation of endogenous repair has been proposed in cell therapy studies (Malliaras et al., 2012, Tang et al., 2010). This correlates with our findings that CPC transplantation increases vascular density and proliferation rate of resident cardiomyocytes. Our main hypothesis that miR-133a enhances CPCs-paracrine effects is supported by the upregulation of *bFgf* and *Vegf* in miR-133-CPCs upon oxidative stress, which might be an indirect consequence of the increased survival of CPCs. In the EHM model, we found that both growth factors were identically upregulated in the CPCs, as well as we found increased levels of *Igf-1* and *Hgf*, being this last factor recently described as protective for hepatic stem cell/progenitor populations subjected to oxidative stress-induced apoptosis (Martínez-Palacián et al., 2013). In the EHM, CPCs were retained during culture, and the addition of miR-133a-CPCs enhanced the contractile capacity. This is at least partially achieved by reduced cardiomyocyte cell death during the initial 3 days of EHM culture and a probable direct effect of increased secretion of *Vegf*, *bFgf*, and *Igf1* on contractility promotion (Cilvik et al., 2013, Troncoso et al., 2014, Zentilin et al., 2010). The first 3 days of EHM culture represent a vulnerable phase accompanied by substantial cell death, mainly by apoptosis of cardiomyocytes (Tiburcy et al., 2011). Antiapoptotic factors are particularly helpful during this early EHM culture phase (Naito et al., 2006, Vantler et al., 2010). Compared with miR-control-CPCs, miR-133a-CPCs reduced cardiomyocyte apoptosis and enabled a higher percentage of cardiomyocytes in longer cultures. Interestingly, inclusion of unmodified CPCs also provided protection, resulting in lower rates of apoptosis (~15%) when compared with standard EHM cultures without CPCs (~35%) (Tiburcy et al., 2011). These lower rates may be explained by the increased expression of cardioprotective growth factors (e.g., *Igf-1*), which are at least partly responsible for the beneficial effects of CSCs/CPCs and MSCs transplanted into ischemic heart (Malliaras et al., 2012, Wang et al., 2009). Other prosurvival factor incremented in miR-133a-EHM was *S100a4*, which has been shown to promote protection against apoptosis and improve cell survival rate in injured myocardium (Schneider et al., 2007). Our own data with the EHM model appear to concur with all of these favorable effects.

Our findings showing an increase of growth factors expression in miR133-CPCs upon stress conditioning and the amelioration of cardiac functions after miR133-CPCs transplantation post-AMI are in agreement with a recent publication that demonstrates that previous supplementation ("priming") of $SCA1^+/CD31^+$ cells with recombinant IGF-1+HGF increases their engraftment capacity and survival rate, promoting angiogenesis and favoring regeneration in response to the hostile microenvironment of an

infarcted heart, after their transplantation (Wang et al., 2014). Our results demonstrate that miR-133a, without affecting proliferation/differentiation potential, promotes CPCs survival and significantly increases their capacity to protect the heart against hypertrophy and apoptosis after MI. Recently, it has been proposed that exosomes, which resulted to be highly enriched in specific miRNAs, play a critical role in hCPC-driven improvement of cardiac function after injury (Barile et al., 2014). Exosomes secreted by CDCs also contain a distinctive repertoire of miRNAs (Ibrahim et al., 2014) and inhibit apoptosis and promote proliferation of cardiomyocytes, while enhancing angiogenesis. All of these recent evidences support the phenotype that we observed with miR-133a-CPCs. We confirmed that secreted miR-133a was mainly incorporated into the exosomal fraction of miR-133a-CPCs-CM, suggesting that direct transfer of the miRNA might mediate part of miR-133a-CPCs paracrine actions on the damaged tissue. However, the high levels of miR-133a already present in mature cardiomyocytes makes unlikely that CPC-exosomal contribution of miR-133a may provide additional significant effects on damaged cardiomyocytes.

Finally, it has been recently demonstrated that the combination of miR-133a with cardiac core transcriptional factors (*Gata4*, *Mef2c*, and *Tbx5*) or GMT plus *Mesp1* and *Myocd* significantly improves direct cardiac reprogramming from human and mouse fibroblasts (Muraoka et al., 2014). Our results on the role of miR-133a in CPCs could be fully compatible with its plausible contribution to transient progenitor survival during the reprogramming process.

In summary, we believe that miR-133a protective actions integrate the rescue of endogenous CPCs, early activated progenitors as angioblasts (Malliaras et al., 2014) or endothelial cells, and the secretome/exosome-mediated repair of damaged resident cardiomyocytes via a complex combination of secreted miRNAs and growth and survival factors. Our work provides a detailed dissection of the mechanisms activated by miR-133-CPC transplantation and establishes the basis for a future improvement of therapeutic use of CPCs for regenerating injured myocardium after infarct.

EXPERIMENTAL PROCEDURES

In Vitro Experiments with CPCs

Adult mouse hearts (C57BL/6 mice, 8–12 weeks old) were treated with collagenase type II (Worthington), and SCA-1$^+$ Lin$^-$ cells were isolated using a Lineage Depletion kit and Sca-1 microbeads (Miltenyi Biotech). For preparation of CM, cardiomyocytes were cultured for 48 hr in fetal bovine serum-free M199 (apoptosis and hypertrophy experiments). For apoptosis experiments, cells were treated for 1–5 hr with 200 μmol/l H_2O_2, and samples were collected for gene expression analysis (RT-PCR) or apoptosis quantification (caspase 3/caspase 9; MBL International).

miR-1 and miR-133a Overexpression

pLenti4 lentiviral vectors were subcloned with the Gateway system (Invitrogen) from pcDNA vectors obtained with a BLOCK-iT Pol II miR RNAi Expression Vector Kit with EmGFP (Invitrogen) and designed for the expression of miR-1, miR-133a, and a nontargeting control miRNA. Retroviral vectors (MiR-Vec) used for the expression of miR-133a, and a control-miRNA, were purchased from Geneservice (Source BioScience). The pRRL.CMV.IRES.GFP lentiviral vector was used to trace GFP$^+$ cells. Supernatants containing lentiviral or retroviral particles were obtained at high titer at the CNIC Viral Vector Facility.

EHM Cultures

EHM culture is a biomimetic in vitro heart model with cardiac muscle properties. EHM cocultures were prepared with CPCs and enriched NRCMs (1:3 ratio, total 2.5 × 10^6 cells per EHM) and maintained as previously described (Tiburcy et al., 2011, Zimmermann et al., 2000, 2002).

Statistical Analysis

Data are generally expressed as mean ± SEM. Data were analyzed with Student's t test for paired experiments and with two-way ANOVA for multiple group comparisons. Analyses were conducted with GraphPad Prism 5.0, and values of $p < 0.05$ were considered statistically significant.

SUPPLEMENTAL INFORMATION

Supplemental Information includes Supplemental Experimental Procedures, seven figures, and four tables and can be found with this article online at http://dx.doi.org/10.1016/j.stemcr.2014.10.010.

AUTHOR CONTRIBUTIONS

A.I. and I.M. performed most of the experimental research; I.V., V.B., and A.D.-J. collaborated in several stages of the initial characterization on CPC populations. S.C. has collaborated in the final experiments requested by reviewers and manuscript adaptation; E.L., M.T., and W.-H.Z. designed and developed the EHM studies. I.J.N.-G., I.C., A.R.-S., and P.S., were involved in the analyses of CPC activity in the murine models of acute cardiac infarct. A.B. coordinated the study and was responsible for manuscript writing and fund raising.

ACKNOWLEDGMENTS

This work was supported by grants to A.B. from the Ministry of Economy and Competition (SAF2012-3432, PLE2009-0147, and PSE-010000-2009-3), the Comunidad Autónoma de Madrid (S2011/BMD-2420), ISCIII (RD12/0019/0018). W.-H.Z. is supported by the DZHK (German Center for Cardiovascular Research), the German Federal Ministry for Science and Education (BMBF FKZ 13GW0007A, joint program with the California Institute of Renerative Medicine), the German Research Foundation (DFG ZI 708/7-1, 8-1, 10-1, SFB 1002 TP C04 and TP S), and the NIH (U01 HL099997). A.B. and W.-H.Z. have been both supported by the European Commission (FP7-HEALTH-2009/CARE-MI). A.I.

and I.M. were postdoctoral fellows funded by the Ministry of Economy and Competition. S.C. is a contracted scientist funded by ISCIII. The CNIC and CNB are supported by the Ministry of Economy and Competition. We thank Iria Sánchez, Tamara Córdoba, Erica López, and Carmen Albo for technical help, Candelas Carreiro for logistics support, Marta Ramón for secretarial assistance, and Kenneth McCreath for help with manuscript editing.

Received: May 20, 2014
Revised: October 20, 2014
Accepted: October 21, 2014
Published: November 20, 2014

REFERENCES

Alcendor, R.R., Gao, S., Zhai, P., Zablocki, D., Holle, E., Yu, X., Tian, B., Wagner, T., Vatner, S.F., and Sadoshima, J. (2007). Sirt1 regulates aging and resistance to oxidative stress in the heart. Circ. Res. *100*, 1512–1521.

Bang, C., Batkai, S., Dangwal, S., Gupta, S.K., Foinquinos, A., Holzmann, A., Just, A., Remke, J., Zimmer, K., Zeug, A., et al. (2014). Cardiac fibroblast-derived microRNA passenger strand-enriched exosomes mediate cardiomyocyte hypertrophy. J. Clin. Invest. *124*, 2136–2146.

Barile, L., Lionetti, V., Cervio, E., Matteucci, M., Gherghiceanu, M., Popescu, L.M., Torre, T., Siclari, F., Moccetti, T., and Vassalli, G. (2014). Extracellular vesicles from human cardiac progenitor cells inhibit cardiomyocyte apoptosis and improve cardiac function after myocardial infarction. Cardiovasc. Res. *103*, 530–541.

Beltrami, A.P., Barlucchi, L., Torella, D., Baker, M., Limana, F., Chimenti, S., Kasahara, H., Rota, M., Musso, E., Urbanek, K., et al. (2003). Adult cardiac stem cells are multipotent and support myocardial regeneration. Cell *114*, 763–776.

Carè, A., Catalucci, D., Felicetti, F., Bonci, D., Addario, A., Gallo, P., Bang, M.L., Segnalini, P., Gu, Y., Dalton, N.D., et al. (2007). MicroRNA-133 controls cardiac hypertrophy. Nat. Med. *13*, 613–618.

Chen, T., Ding, G., Jin, Z., Wagner, M.B., and Yuan, Z. (2012). Insulin ameliorates miR-1-induced injury in H9c2 cells under oxidative stress via Akt activation. Mol. Cell. Biochem. *369*, 167–174.

Chen, S., Puthanveetil, P., Feng, B., Matkovich, S.J., Dorn, G.W., 2nd, and Chakrabarti, S. (2014). Cardiac miR-133a overexpression prevents early cardiac fibrosis in diabetes. J. Cell. Mol. Med. *18*, 415–421.

Cheng, C., Wang, Q., You, W., Chen, M., and Xia, J. (2014). MiRNAs as biomarkers of myocardial infarction: a meta-analysis. PLoS ONE *9*, e88566.

Chugh, A.R., Beache, G.M., Loughran, J.H., Mewton, N., Elmore, J.B., Kajstura, J., Pappas, P., Tatooles, A., Stoddard, M.F., Lima, J.A., et al. (2012). Administration of cardiac stem cells in patients with ischemic cardiomyopathy: the SCIPIO trial: surgical aspects and interim analysis of myocardial function and viability by magnetic resonance. Circulation *126* (11, Suppl 1), S54–S64.

Cilvik, S.N., Wang, J.I., Lavine, K.J., Uchida, K., Castro, A., Gierasch, C.M., Weinheimer, C.J., House, S.L., Kovacs, A., Nichols, C.G., and Ornitz, D.M. (2013). Fibroblast growth factor receptor 1 signaling in adult cardiomyocytes increases contractility and results in a hypertrophic cardiomyopathy. PLoS ONE *8*, e82979.

Cottini, F., Hideshima, T., Xu, C., Sattler, M., Dori, M., Agnelli, L., ten Hacken, E., Bertilaccio, M.T., Antonini, E., Neri, A., et al. (2014). Rescue of Hippo coactivator YAP1 triggers DNA damage-induced apoptosis in hematological cancers. Nat. Med. *20*, 599–606.

Danowski, N., Manthey, I., Jakob, H.G., Siffert, W., Peters, J., and Frey, U.H. (2013). Decreased expression of miR-133a but not of miR-1 is associated with signs of heart failure in patients undergoing coronary bypass surgery. Cardiology *125*, 125–130.

Del Re, D.P., Matsuda, T., Zhai, P., Maejima, Y., Jain, M.R., Liu, T., Li, H., Hsu, C.P., and Sadoshima, J. (2014). Mst1 promotes cardiac myocyte apoptosis through phosphorylation and inhibition of Bcl-xL. Mol. Cell *54*, 639–650.

Deng, Z., Chen, J.F., and Wang, D.Z. (2011). Transgenic overexpression of miR-133a in skeletal muscle. BMC Musculoskelet. Disord. *12*, 115.

Galvez, B.G., Sampaolesi, M., Barbuti, A., Crespi, A., Covarello, D., Brunelli, S., Dellavalle, A., Crippa, S., Balconi, G., Cuccovillo, I., et al. (2008). Cardiac mesoangioblasts are committed, self-renewable progenitors, associated with small vessels of juvenile mouse ventricle. Cell Death Differ. *15*, 1417–1428.

Gao, S., Wassler, M., Zhang, L., Li, Y., Wang, J., Zhang, Y., Shelat, H., Williams, J., and Geng, Y.J. (2014). MicroRNA-133a regulates insulin-like growth factor-1 receptor expression and vascular smooth muscle cell proliferation in murine atherosclerosis. Atherosclerosis *232*, 171–179.

He, B., Xiao, J., Ren, A.J., Zhang, Y.F., Zhang, H., Chen, M., Xie, B., Gao, X.G., and Wang, Y.W. (2011). Role of miR-1 and miR-133a in myocardial ischemic postconditioning. J. Biomed. Sci. *18*, 22.

Hori, M., and Nishida, K. (2009). Oxidative stress and left ventricular remodelling after myocardial infarction. Cardiovasc. Res. *81*, 457–464.

Hu, S., Huang, M., Nguyen, P.K., Gong, Y., Li, Z., Jia, F., Lan, F., Liu, J., Nag, D., Robbins, R.C., and Wu, J.C. (2011). Novel microRNA prosurvival cocktail for improving engraftment and function of cardiac progenitor cell transplantation. Circulation *124* (11, Suppl.), S27–S34.

Hullinger, T.G., Montgomery, R.L., Seto, A.G., Dickinson, B.A., Semus, H.M., Lynch, J.M., Dalby, C.M., Robinson, K., Stack, C., Latimer, P.A., et al. (2012). Inhibition of miR-15 protects against cardiac ischemic injury. Circ. Res. *110*, 71–81.

Ibrahim, A.G., Cheng, K., and Marbán, E. (2014). Exosomes as critical agents of cardiac regeneration triggered by cell therapy. Stem Cell Rep. *2*, 606–619.

Ivey, K.N., and Srivastava, D. (2010). MicroRNAs as regulators of differentiation and cell fate decisions. Cell Stem Cell *7*, 36–41.

Ivey, K.N., Muth, A., Arnold, J., King, F.W., Yeh, R.F., Fish, J.E., Hsiao, E.C., Schwartz, R.J., Conklin, B.R., Bernstein, H.S., and Srivastava, D. (2008). MicroRNA regulation of cell lineages in mouse and human embryonic stem cells. Cell Stem Cell *2*, 219–229.

Jiang, Y., Zhang, M., He, H., Chen, J., Zeng, H., Li, J., and Duan, R. (2013). MicroRNA/mRNA profiling and regulatory network of intracranial aneurysm. BMC Med. Genomics *6*, 36.

Labi, V., Bertele, D., Woess, C., Tischner, D., Bock, F.J., Schwemmers, S., Pahl, H.L., Geley, S., Kunze, M., Niemeyer, C.M., et al. (2013). Haematopoietic stem cell survival and transplantation efficacy is limited by the BH3-only proteins Bim and Bmf. EMBO Mol. Med. *5*, 122–136.

Lee, R., Feinbaum, R., and Ambros, V. (2004). A short history of a short RNA. Cell *116*, S89–92, 1 p following S96.

Li, Z., Hassan, M.Q., Volinia, S., van Wijnen, A.J., Stein, J.L., Croce, C.M., Lian, J.B., and Stein, G.S. (2008). A microRNA signature for a BMP2-induced osteoblast lineage commitment program. Proc. Natl. Acad. Sci. USA *105*, 13906–13911.

Liao, X.B., Zhang, Z.Y., Yuan, K., Liu, Y., Feng, X., Cui, R.R., Hu, Y.R., Yuan, Z.S., Gu, L., Li, S.J., et al. (2013). MiR-133a modulates osteogenic differentiation of vascular smooth muscle cells. Endocrinology *154*, 3344–3352.

Liu, N., Bezprozvannaya, S., Williams, A.H., Qi, X., Richardson, J.A., Bassel-Duby, R., and Olson, E.N. (2008). microRNA-133a regulates cardiomyocyte proliferation and suppresses smooth muscle gene expression in the heart. Genes Dev. *22*, 3242–3254.

Malliaras, K., Li, T.S., Luthringer, D., Terrovitis, J., Cheng, K., Chakravarty, T., Galang, G., Zhang, Y., Schoenhoff, F., Van Eyk, J., et al. (2012). Safety and efficacy of allogeneic cell therapy in infarcted rats transplanted with mismatched cardiosphere-derived cells. Circulation *125*, 100–112.

Malliaras, K., Makkar, R.R., Smith, R.R., Cheng, K., Wu, E., Bonow, R.O., Marbán, L., Mendizabal, A., Cingolani, E., Johnston, P.V., et al. (2014). Intracoronary cardiosphere-derived cells after myocardial infarction: evidence of therapeutic regeneration in the final 1-year results of the CADUCEUS trial (CArdiosphere-Derived aUtologous stem CElls to reverse ventricULar dySfunction). J. Am. Coll. Cardiol. *63*, 110–122.

Martínez-Palacián, A., del Castillo, G., Suárez-Causado, A., García-Álvaro, M., de Morena-Frutos, D., Fernández, M., Roncero, C., Fabregat, I., Herrera, B., and Sánchez, A. (2013). Mouse hepatic oval cells require Met-dependent PI3K to impair TGF-β-induced oxidative stress and apoptosis. PLoS ONE *8*, e53108.

Matkovich, S.J., Wang, W., Tu, Y., Eschenbacher, W.H., Dorn, L.E., Condorelli, G., Diwan, A., Nerbonne, J.M., and Dorn, G.W., 2nd. (2010). MicroRNA-133a protects against myocardial fibrosis and modulates electrical repolarization without affecting hypertrophy in pressure-overloaded adult hearts. Circ. Res. *106*, 166–175.

Moscoso, I., Tejados, N., Barreiro, O., Sepúlveda, P., Izarra, A., Calvo, E., Dorronsoro, A., Salcedo, J.M., Sádaba, R., Díez-Juan, A., et al. (2013). Podocalyxin-like protein 1 is a relevant marker for human c-kit(pos) cardiac stem cells. J. Tissue Eng. Regen. Med. Published online July 30, 2013. http://dx.doi.org/10.1002/term.1795.

Muraoka, N., Yamakawa, H., Miyamoto, K., Sadahiro, T., Umei, T., Isomi, M., Nakashima, H., Akiyama, M., Wada, R., Inagawa, K., et al. (2014). MiR-133 promotes cardiac reprogramming by directly repressing Snai1 and silencing fibroblast signatures. EMBO J. *33*, 1565–1581.

Naito, H., Melnychenko, I., Didié, M., Schneiderbanger, K., Schubert, P., Rosenkranz, S., Eschenhagen, T., and Zimmermann, W.H. (2006). Optimizing engineered heart tissue for therapeutic applications as surrogate heart muscle. Circulation *114* (1 Suppl.), I72–I78.

Oh, H., Bradfute, S.B., Gallardo, T.D., Nakamura, T., Gaussin, V., Mishina, Y., Pocius, J., Michael, L.H., Behringer, R.R., Garry, D.J., et al. (2003). Cardiac progenitor cells from adult myocardium: homing, differentiation, and fusion after infarction. Proc. Natl. Acad. Sci. USA *100*, 12313–12318.

Piñon, J.D., Labi, V., Egle, A., and Villunger, A. (2008). Bim and Bmf in tissue homeostasis and malignant disease. Oncogene *27* (*Suppl 1*), S41–S52.

Puthanveetil, P., Wan, A., and Rodrigues, B. (2013). FoxO1 is crucial for sustaining cardiomyocyte metabolism and cell survival. Cardiovasc. Res. *97*, 393–403.

Robey, T.E., Saiget, M.K., Reinecke, H., and Murry, C.E. (2008). Systems approaches to preventing transplanted cell death in cardiac repair. J. Mol. Cell. Cardiol. *45*, 567–581.

Sanganalmath, S.K., and Bolli, R. (2013). Cell therapy for heart failure: a comprehensive overview of experimental and clinical studies, current challenges, and future directions. Circ. Res. *113*, 810–834.

Schneider, M., Kostin, S., Strøm, C.C., Aplin, M., Lyngbaek, S., Theilade, J., Grigorian, M., Andersen, C.B., Lukanidin, E., Lerche Hansen, J., and Sheikh, S.P. (2007). S100A4 is upregulated in injured myocardium and promotes growth and survival of cardiac myocytes. Cardiovasc. Res. *75*, 40–50.

Takaya, T., Ono, K., Kawamura, T., Takanabe, R., Kaichi, S., Morimoto, T., Wada, H., Kita, T., Shimatsu, A., and Hasegawa, K. (2009). MicroRNA-1 and MicroRNA-133 in spontaneous myocardial differentiation of mouse embryonic stem cells. Circ. J. *73*, 1492–1497.

Tang, X.L., Rokosh, G., Sanganalmath, S.K., Yuan, F., Sato, H., Mu, J., Dai, S., Li, C., Chen, N., Peng, Y., et al. (2010). Intracoronary administration of cardiac progenitor cells alleviates left ventricular dysfunction in rats with a 30-day-old infarction. Circulation *121*, 293–305.

Tateishi, K., Ashihara, E., Takehara, N., Nomura, T., Honsho, S., Nakagami, T., Morikawa, S., Takahashi, T., Ueyama, T., Matsubara, H., and Oh, H. (2007). Clonally amplified cardiac stem cells are regulated by Sca-1 signaling for efficient cardiovascular regeneration. J. Cell Sci. *120*, 1791–1800.

Tiburcy, M., Didié, M., Boy, O., Christalla, P., Döker, S., Naito, H., Karikkineth, B.C., El-Armouche, A., Grimm, M., Nose, M., et al. (2011). Terminal differentiation, advanced organotypic maturation, and modeling of hypertrophic growth in engineered heart tissue. Circ. Res. *109*, 1105–1114.

Townley-Tilson, W.H., Callis, T.E., and Wang, D. (2010). MicroRNAs 1, 133, and 206: critical factors of skeletal and cardiac muscle development, function, and disease. Int. J. Biochem. Cell Biol. *42*, 1252–1255.

Troncoso, R., Ibarra, C., Vicencio, J.M., Jaimovich, E., and Lavandero, S. (2014). New insights into IGF-1 signaling in the heart. Trends Endocrinol. Metab. *25*, 128–137.

Vantler, M., Karikkineth, B.C., Naito, H., Tiburcy, M., Didié, M., Nose, M., Rosenkranz, S., and Zimmermann, W.H. (2010). PDGF-BB protects cardiomyocytes from apoptosis and improves

contractile function of engineered heart tissue. J. Mol. Cell. Cardiol. *48*, 1316–1323.

Wang, X., Zhao, T., Huang, W., Wang, T., Qian, J., Xu, M., Kranias, E.G., Wang, Y., and Fan, G.C. (2009). Hsp20-engineered mesenchymal stem cells are resistant to oxidative stress via enhanced activation of Akt and increased secretion of growth factors. Stem Cells *27*, 3021–3031.

Wang, Y., Li, L., Moore, B.T., Peng, X.H., Fang, X., Lappe, J.M., Recker, R.R., and Xiao, P. (2012). MiR-133a in human circulating monocytes: a potential biomarker associated with postmenopausal osteoporosis. PLoS ONE *7*, e34641.

Wang, X., Li, Q., Hu, Q., Suntharalingam, P., From, A.H., and Zhang, J. (2014). Intra-myocardial injection of both growth factors and heart derived Sca-1+/CD31- cells attenuates post-MI LV remodeling more than does cell transplantation alone: neither intervention enhances functionally significant cardiomyocyte regeneration. PLoS ONE *9*, e95247.

Yildirim, S.S., Akman, D., Catalucci, D., and Turan, B. (2013). Relationship between downregulation of miRNAs and increase of oxidative stress in the development of diabetic cardiac dysfunction: junctin as a target protein of miR-1. Cell Biochem. Biophys. *67*, 1397–1408.

Zentilin, L., Puligadda, U., Lionetti, V., Zacchigna, S., Collesi, C., Pattarini, L., Ruozi, G., Camporesi, S., Sinagra, G., Pepe, M., et al. (2010). Cardiomyocyte VEGFR-1 activation by VEGF-B induces compensatory hypertrophy and preserves cardiac function after myocardial infarction. FASEB J. *24*, 1467–1478.

Zhao, Y., Samal, E., and Srivastava, D. (2005). Serum response factor regulates a muscle-specific microRNA that targets Hand2 during cardiogenesis. Nature *436*, 214–220.

Zhao, Y., Ransom, J.F., Li, A., Vedantham, V., von Drehle, M., Muth, A.N., Tsuchihashi, T., McManus, M.T., Schwartz, R.J., and Srivastava, D. (2007). Dysregulation of cardiogenesis, cardiac conduction, and cell cycle in mice lacking miRNA-1-2. Cell *129*, 303–317.

Zimmermann, W.H., Fink, C., Kralisch, D., Remmers, U., Weil, J., and Eschenhagen, T. (2000). Three-dimensional engineered heart tissue from neonatal rat cardiac myocytes. Biotechnol. Bioeng. *68*, 106–114.

Zimmermann, W.H., Schneiderbanger, K., Schubert, P., Didié, M., Münzel, F., Heubach, J.F., Kostin, S., Neuhuber, W.L., and Eschenhagen, T. (2002). Tissue engineering of a differentiated cardiac muscle construct. Circ. Res. *90*, 223–230.

Stem Cell Reports, Volume *3*

Supplemental Information

miR-133a Enhances the Protective Capacity of Cardiac Progenitors Cells after Myocardial Infarction

Alberto Izarra, Isabel Moscoso, Elif Levent, Susana Cañón, Inmaculada Cerrada, Antonio Díez-Juan, Vanessa Blanca, Iván-J. Núñez-Gil, Iñigo Valiente, Amparo Ruíz-Sauri, Pilar Sepúlveda, Malte Tiburcy, Wolfram-H. Zimmermann, and Antonio Bernad

SUPPLEMENTAL FIGURE AND LEGENDS

Supplemental Figure 1

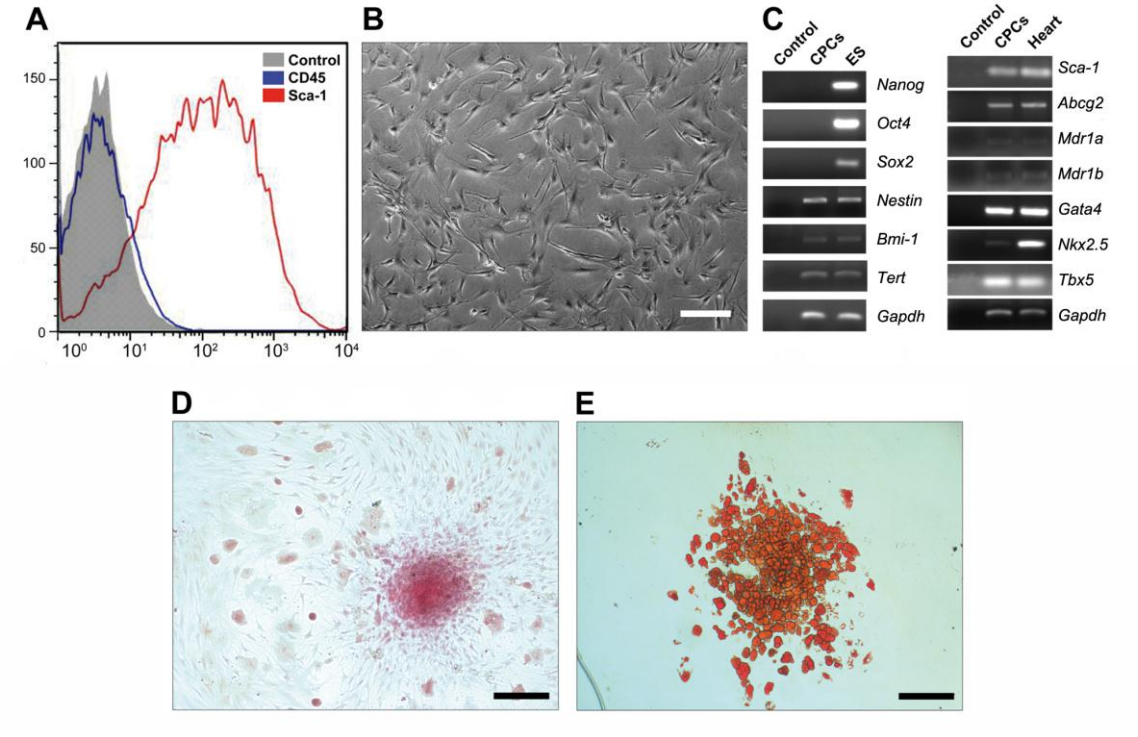

Figure S1. Characterization of CPCs. A, CPCs SCA-1^+/$CD45^-$ FACS characterization. B, Bright-field morphology of cultured CPCs. C, Expression profile (RT-PCR) of stem cell- and cardiac-related genes. D,E, Differentiation potential of SCA-1^+/$CD45^-$ CPCs. Cells were treated with differentiation medium for D, osteocytes or E, adipocytes, and stained with Alizarin Red and Oil Red O, respectively (bar, 200 μm).

Supplemental Figure 2

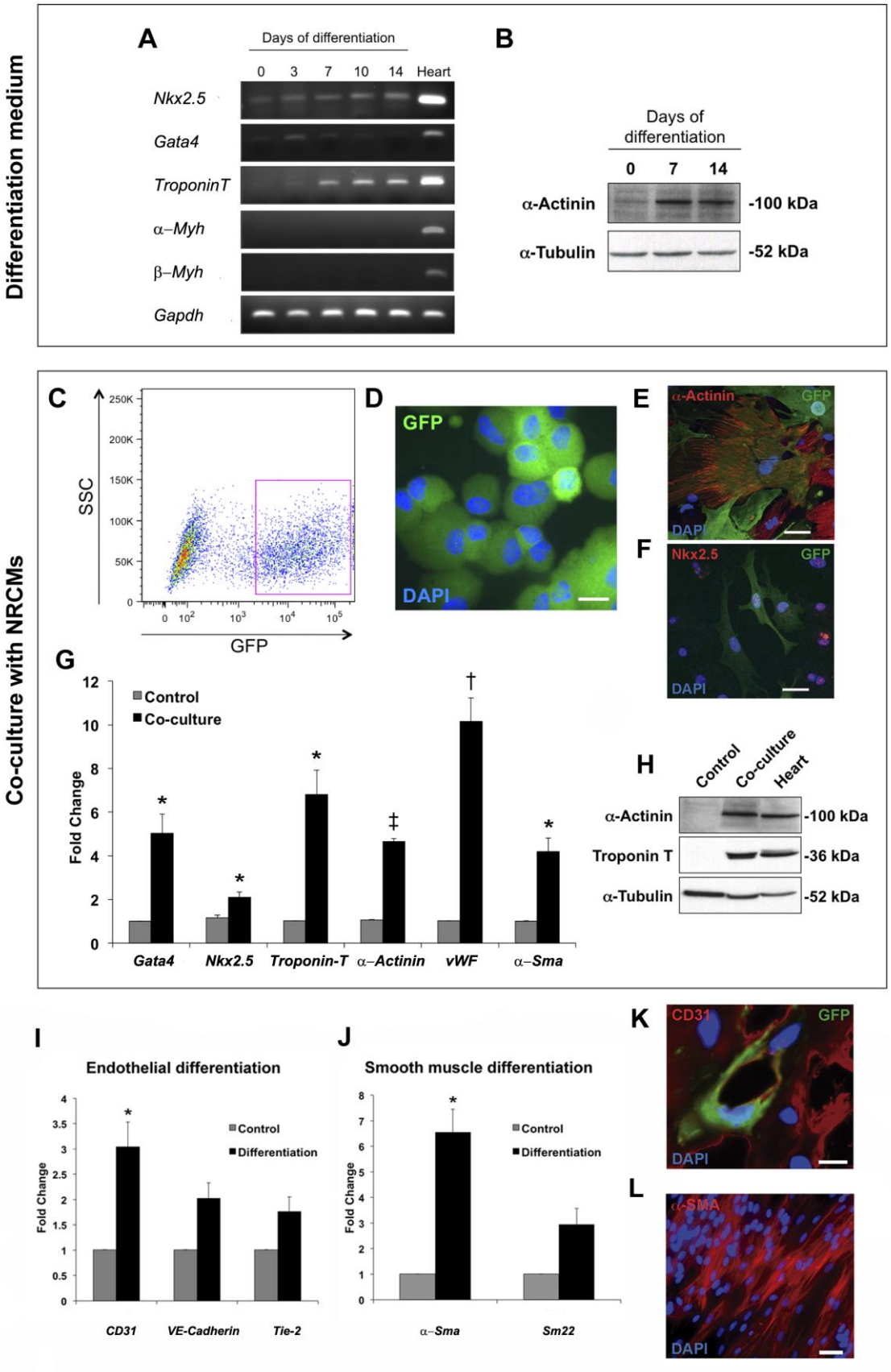

Figure S2. CPC differentiation. A, RT-PCR analysis of *Nkx2.5*, *Gata4*, *Troponin T*, *α-Myh* and *β-Myh* expression after culture of CPC-derived GFP^+cells in cardiac differentiation medium. Troponin T is detectable from day 7 of differentiation. Heart was used a positive control. B, Western blot analysis of α-actinin during cardiac-induced differentiation. α-actinin is detectable from day 7 of differentiation. C, CPC-derived GFP^+cells were isolated from co-cultures with NRCMs by FACS. D, GFP expression was validated by cytospin followed by microscopy (bar, 20 μm). E, F, GFP^+ CPCs were seeded with NRCMs, and after co-culture for 7 days, some GFP^+ CPC-derived cells stained positive for α-actinin (E) and NKX2.5 (F) (bars, 40 μm). G, Quantitative RT-PCR analysis of cardiac (*Gata4, Nkx2.5, Troponin T* and *α-Actinin*) and endothelial (*von Willebrand factor (vWf)* and *α-Sma*) gene expression in FACS-purified GFP^+-CPCs from control cultures and from NRCM co-cultures (n=3 experiments). H, Representative Western blot analysis of troponin T and α-actinin in control CPCs and CPCs isolated from NRCM co-cultures. Heart was used a positive control. I, RT-qPCR analysis of *CD31*, *VE-cadherin* and *Tie2* expression in control CPCs and endothelial-differentiated CPCs (n=3 experiments). J, RT-qPCR analysis of endothelial *α-Sma* and *Sm22* expression in control CPCs and smooth muscle-differentiated CPCs (n=3 experiments). $*P<0.05$, $\dagger P<0.01$, $\ddagger P<0.001$. Data are mean±SEM. K, GFP^+ CPC-derived endothelial cells express CD31 after *in vivo* angiogenesis plug assay (bar, 20 μm). L, CPC-derived smooth muscle cells express α-SMA after differentiation in specific medium (bar, 40 μm).

Supplemental Figure 3

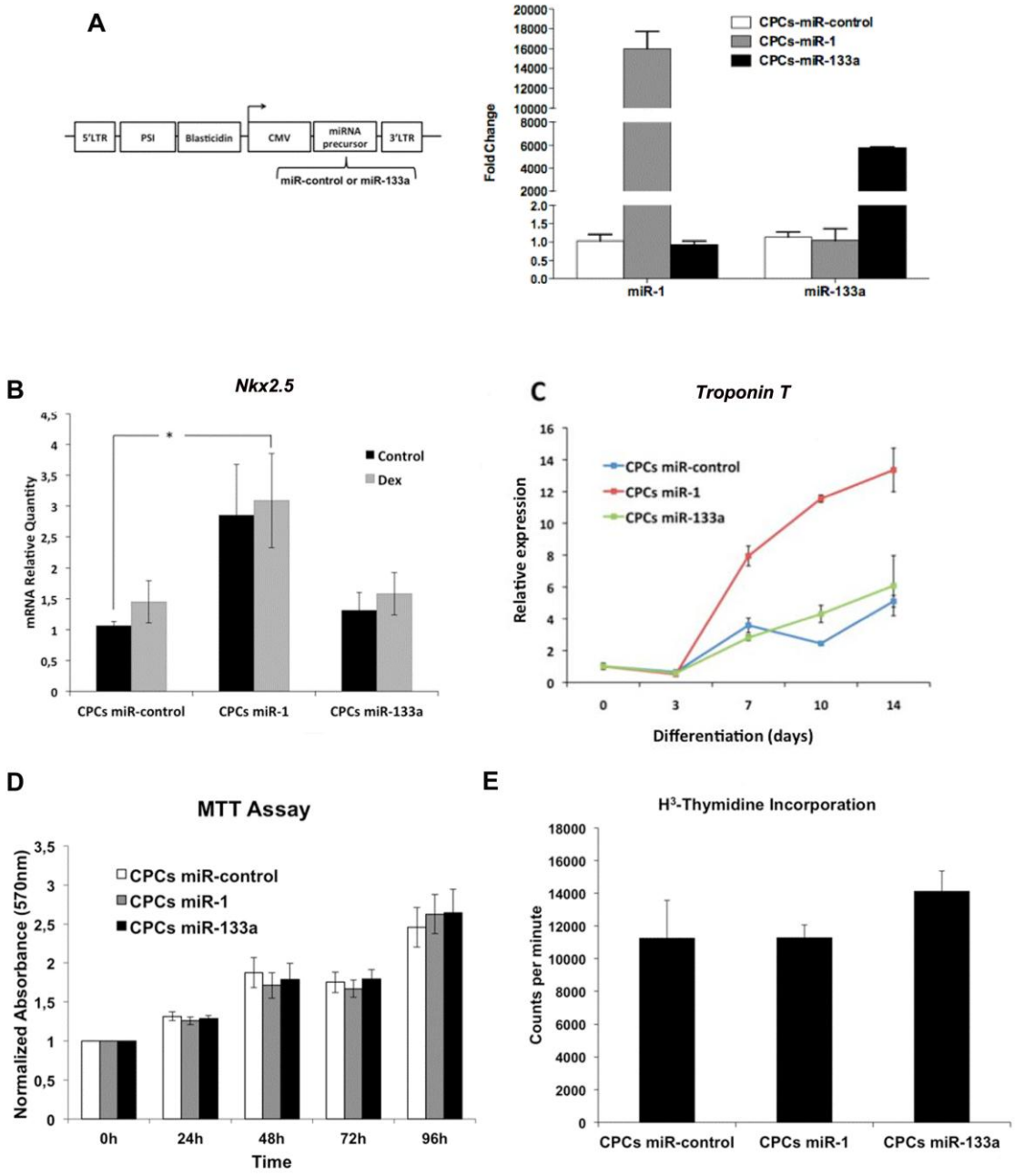

Figure S3. Effect of miR-1 and miR-133a overexpression on CPC differentiation and proliferation. Related to Fig 1. A, Retroviral vector used for overexpression of miR-1 miR-133a and miR-control (left); quantitative analysis of miRNA overexpression in CPCs (right, n=3 experiments). B, RT-qPCR expression analysis of *Nkx2.5* in undifferentiated *versus* CPCs cultured in differentiation medium (n=3 experiments). C,

Representative time-course RT-qPCR analysis of *troponin T* expression after induction of differentiation (n=3 experiments). D, Colorimetric MTT assay over 96 hours (n=2 experiments; n=3 replicates per condition). E, ^{3}H-thymidine incorporation assay at 48 hours (n=3 experiments). **P*<0.05. Data are represented as mean±SEM. Related to Fig 1.

Supplemental Figure 4

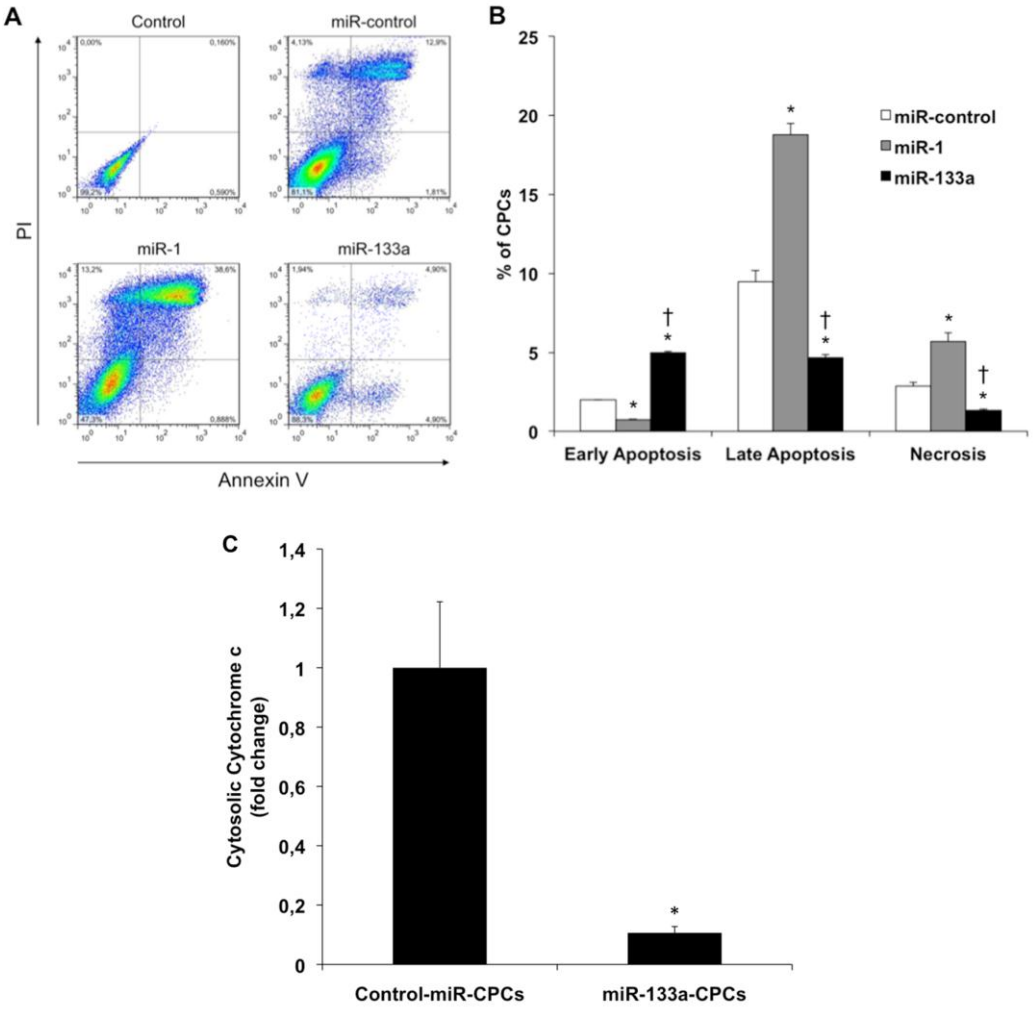

Figure S4. Effect of miR-1 and miR-133a overexpression on CPC apoptosis. Related to Fig 1. A, Representative FACS analysis of CPCs treated with H_2O_2 (200μM; 5 hours) and stained with annexin V and PI. B, Quantification of early apoptosis (annexin V^+/PI^- cells), late apoptosis (Annexin V^+/PI^+ cells) and necrosis (annexin V^-/PI^+ cells) after H_2O_2 treatment (n=3 experiments; **P*<0.05 respect to miR-control, †*P*<0.005 respect to miR-1). C, Fold change quantification of cytosolic cytochrome c in CPCs after H_2O_2 treatment (n=3 experiments; **P*<0.05). Data are represented as mean±SEM. Related to Fig 1.

Supplemental Figure 5

A

Category	Functions	Functions Annotation	p-Value	# Molecules
Cell Death	cell death	cell death	**9,19E-13**	319
Cell Death	apoptosis	apoptosis	**4,27E-11**	248
Cardiovascular Disease	heart disease	heart disease	**2,67E-09**	164
Cell Death	cell death	cell death of organ	**1,55E-08**	106
Cardiovascular Disease	ischemia	ischemia	**2,96E-07**	130

B

Category	Diseases/Functions Annotation	p-Value	Molecules
Cell Death/ Survival	cell death	**4.61E-19**	353
Cell Death/ Survival	apoptosis	**1.07E-17**	289
Cell Death/ Survival	necrosis	**5.63E-15**	277
Cell Death/ Survival	neuronal cell death	**4.68E-09**	80
Cell Death/ Survival	apoptosis of neurons	**2.26E-08**	55
Cell Death/ Survival	cell death of brain cells	**2.91E-07**	36
Cell Death/ Survival	cell death of tumor cell lines	**3.07E-07**	157
Cell Death/ Survival	cell death of central nervous system cells	**3.26E-07**	38
Cell Death/ Survival	cell death of connective tissue cells	**6.53E-07**	71
Cell Death/ Survival [1]	cell death of blood cells	**1.51E-06**	75
Cell Death/ Survival	apoptosis of tumor cell lines	**4.90E-06**	122
Cell Death/ Survival	cell death of fibroblasts	**1.27E-05**	32
Cell Death/ Survival	cell death of immune cells	**1.53E-05**	69
Cell Death/ Survival	apoptosis of connective tissue cells	5.91E-05	33
Cell Death/ Survival [1]	cell death hematopoietic progenitor cells	**6.05E-05**	28

[1] *Abcc1,Adcyap1,**Adora2a**,Alk,Arrb1,**Bcl2l1,Bcl2l11,Bmf,Bnip3l**,Camk2g,Ccnd2,Cd300a,Cd4,**Cdc42, Cflar**,Cnr1,Cnr2,**Col1a1,Csf2**,Dapk2,Def6,Dicer1,**Dnaja3,E2f1**,Egfr,Ezr,F2r,**Faim**,Fcgr1a,Fcgr3a, Fgfr1,**Fli1,Fnip1**,Foxo1,Gcnt1,**Gimap1,Gimap5,Hrk**,Ikbke,Il6r,Inpp5d,Irak3,Irf2,Itga4,Itga5,Itpkb,Klrc4-Klrk1,Klrk1,Ltbr,Mapk3,**Meis1,Mt1e,Nf1,Nfat5,Nfatc2,Nfya**,Nlrp3,**Notch1**,Npc1,**Nr5a1,Perp,Pml**, Prdx6,Prkcd,Rras,Sh3bp2,Sirpa,**Slc46a1**,Slc6a6,Smad6,Syk,**Tcf7,Thpo**,Trem1,Vdr,Vipr2a,**Wnt5a***

C

Category	Diseases or Functions Annotation	p-Value	Molecules
Cardiac Proliferation [2]	proliferation of heart cells	**1.43E-03**	11
Cardiac Proliferation [2]	proliferation of cardiomyocytes	**1.85E-03**	10
Cardiac Arrythmia	bradycardia	**5.02E-03**	6
Cardiac Proliferation	proliferation of ventricular myocytes	**8.18E-03**	3
Cardiac Arrythmia	arrhythmia	**8.80E-03**	20
Cardiac Fibrosis [3]	fibrosis of heart	**1.08E-02**	12
Cardiac Arrythmia	supraventricular arrhythmia	**1.12E-02**	14
Cardiac Arrythmia	arrhythmia of heart ventricle	**1.17E-02**	9
Cardiac Arrythmia	paroxysmal supraventr. tachycardia	**1.40E-02**	5
Cardiac Necrosis/Cell Death [4]	apoptosis of cardiomyocytes	**1.65E-02**	16
Increased Red Blood Cells	increased quantity of red blood cells	**1.97E-02**	11
Cardiac Fibrosis [3]	fibrosis of left ventricle	**2.83E-02**	4
Cardiac Arrythmia	tachycardia	**3.42E-02**	9
Cardiac Necrosis/Cell Death [4]	cell death of cardiomyocytes	**3.53E-02**	17
Cardiac Necrosis/Cell Death	cell death of heart	**3.68E-02**	18

[2] ***Agt**,Dicer1,**Dusp1,Egfr,Foxo1,Igf2,Mapk11,Meis1,Ncoa6,Nfat5,Rbpj***

[3] *Adora1,**Adra2aA,AgtT**,Cnr2,Dicer1,**Dio3,**Igf1r,Ikbke,Mapk11,Nf1,**Stk4,**Vdr*

[4] ***Adra1a,AgtT,Bcl2l1,Bcl2l11,Bnip3l,**Cnr2,**Dicer1,E2f1,Fstl1,Gnaq,Mtpn,Prkcd,Sirt1,Slc8a1,Sptlc2, Stk4,Ube4b***

Figure S5. Bioinformatics analysis of Top Biological and Toxic Functions involving predicted miR-133a targets. A and B, Bioinformatics analysis of putative Top Disease and Biological Functions affected by miR-133 (IPA analysis software). IPA analysis predicted *cell death* (highlighted in yellow) as the main biological function affected at

organ and cellular levels, followed by *cardiovascular disease* (A). From all genes (106) included in the *cell death* category, we selected those related to injured heart, blood cells and progenitor precursor populations (highlighted in light green) (B). B**[1]**, The total list of genes included in the categories named as *cell death of blood cells* and *cell death of hematopoietic precursors* (genes present in both lists are in bold letter). C, Bioinformatics IPA analysis of putative Top Toxic Functions affected by miR-133. Targets involved in fibrosis and cell death of heart and in proliferation and apoptosis of heart cells and cardiomyocytes, were listed with high p-values. C**[2]**, List of genes included in the categories named as *proliferation of heart cells* and *proliferation of cardiomyocytes* (genes present in both lists are in bold letter). C**[3]**, List of genes included in the categories named as *fibrosis of heart* and *fibrosis of left ventricle* (genes present in both lists are in bold letter). C**[4]**, List of genes included in the categories named as *apoptosis of cardiomyocytes* and *cell death of cardiomyocytes* (genes present in both lists are in bold letter).

Supplemental Figure 6

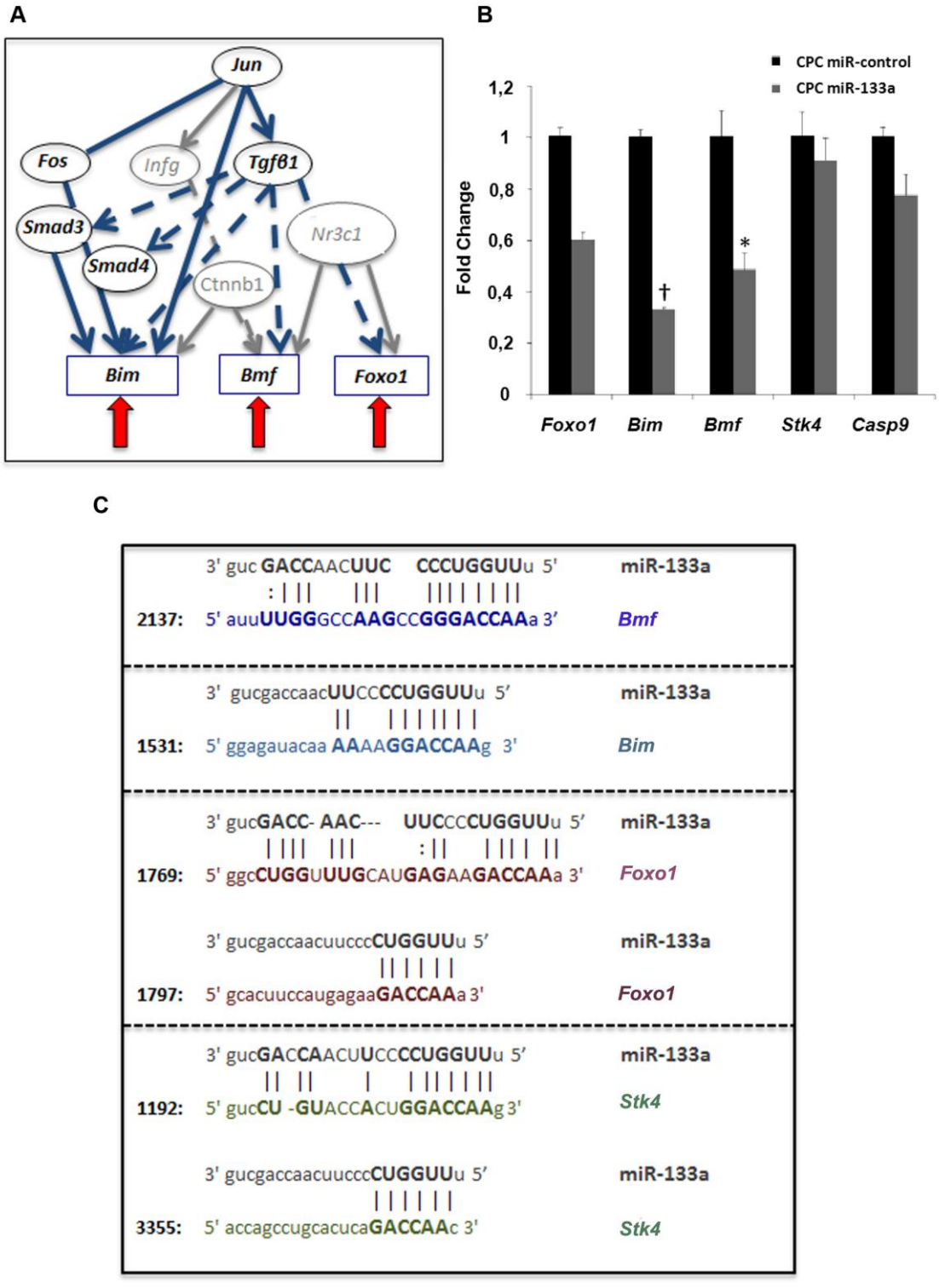

Figure S6. Bioinformatics analysis of predicted up-stream regulator pathways and validation of miR-133 selected targets. Related to Fig 1. A, IPA bioinformatics analysis looking for putative up-stream regulator pathways that could be affected based

on the list of 106 predicted targets list for miR-133a included in cell death category. Solid arrows and lines show direct relationship among genes, dashed-line arrows show indirect relationships among genes, grey shaded arrows and genes are not directly involved in the main pathway highlighted in bold letter, red solid arrows point to predicted activated targets upon activation of the upstream-regulator pathway in bold letter. B, RT-qPCR expression analysis of our target selection in miR-control-CPCs *vs* miR-133a-CPCs, after H_2O_2 treatment; caspase 9 was used as a positive control (5 hours; n=3 experiments; †p<0.00005, *p<0.005). Data are represented as mean±SEM; values are relative to the expression level of the corresponding gene in miR-control-CPCs. C, 3'-UTR binding sites for miR-133a in *Bmf*, *Bim*, *Foxo1* (2 sites) and *Stk4* (2 sites) (obtained from microRNA.org). Related to Fig 1.

Supplemental Figure 7

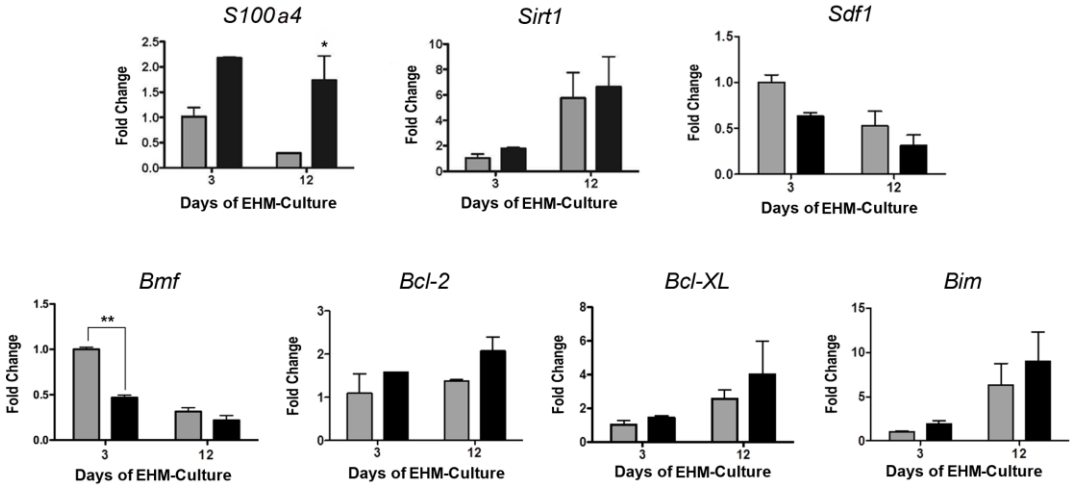

Figure S7. miR-133a-EHM differential expression profile. Related to Fig 7. RT-qPCR expression analysis of *S100a4, Sirt1, Sdf1, Bmf, Bcl-2, Bcl-XL* and *Bim* in control-miR-CPCs (grey bars) and miR-133a-CPCs (black bars) in EHM co-cultures at day 3 and day 12 (n=3 independent experiments, *p<0.05, **p<0.01). Data are represented as mean±SEM.

SUPPLEMENTAL TABLES

Table S1. Primary antibodies. Related to Figures 2, 4, 5, 6 and 7.

Primary Ab	**Manufacturer**	**Species**	**Dilution (application)**
Sarcomeric actin	Dako (M 0874)	Mouse	1:100 (IHC)
CD31	BD Pharmingen (553370)	Rat	1:100 (IF)
CD45-eFluor450	eBioscience (48-0451)	Rat	1:100 (FCyt)
CD45-PE	BD Pharmingen (553081)	Rat	1:100 (FCyt)
GFP	Abcam (ab290)	Rabbit	1:100 (IF)
Laminin	Abcam (ab11575)	Rabbit	1:50 (IF)
NKX2.5	Santa Cruz Biotech (sc-14033)	Rabbit	1:50 (IF/FCyt)
Sca-1-FITC	BD Pharmingen (553335)	Rat	1:20 (FCyt)
Sca-1-PE	BD Pharmingen (553336)	Rat	1:100 (FCyt)
Tropomyosin	Sigma (T2780)	Mouse	1:100 (IF/FCyt)
Troponin T	Abcam (ab8295)	Mouse	1:100 (IF); 1:1000 (WB)
α-SMA	Sigma (A2547)	Mouse	1:1000 (IF)
α-Tubulin	Calbiochem (CP60)	Mouse	1:2000 (WB)

IF: Immunofluorescence. WB: Western blot. FCyt: Flow cytometry.

Table S2. Primers for RT-PCR and real time RT-PCR. Related to Figures 1, 5, 6 and 7.

Primer	**Sense**	**Antisense**
Abcg2	5’-AGCAGCAAGGAAAGATCCAA-3’	5’-CCCATCACAACGTCATCTTG-3’
Bcl-2	5´- GGTCTTCAGAGACAGCCAGG-3´	5´- GATCCAGGATAACGGAGGCT-3´
Bcl-XL	5´- GCTGCATTGTTCCCGTAGAG-3´	5´- GTTGGATGGCCACCTATCTG-3´
bFgf	5’-TTCATAGCAAGGTACCGGTTG-3’	5’-AGAAGAGCGACCCACACG-3’
Bim	5’-GCTCCTGTGCAATCCGTATC-3’	5’-GCCCCTACCTCCCTACAGAC-3’
Bmf	5’-CTGTTCAGGGCGAGGTTTT-3’	5’-AGTTCCATCGGCTTCATACG-3’
Bmi-1	5’-TTTTATGCTGAACGACTTTTAACTT-3’	5’-GCTCAGTGATCTTGATTCTGGT-3’
CD31	5’-AGTTGCTGCCCATTCATCAC-3’	5’-CTGGTGCTCTATGCAAGCCT-3’
Flk-1	5’- TCCAGAATCCTCTTCCATGC-3’	5’- AAACCTCCTGCAAGCAAATG-3’
Gata4	5’-CCATCTCGCCTCCAGAGT-3’	5’-CTGGAAGACACCCCAATCTC-3’
Gfp	5’-CCACATGAAGCAGCACGAC-3’	5’-GTGCTCAGGTAGTGGTTG-3’
Gusb	5’-ACTCCTCACTGAACATGCGA-3’	5’-ATAAGACGCATCAGAAGCCG-3’
Hgf	5’-CTTCTCCTTGGCCTTGAATG-3’	5’-CCTGACACCACTTGGGAGTA-3’
Igf-1	5’-CACTCATCCACAATGCCTGT-3’	5’-TGGATGCTCTTCAGTTCGTG-3’
Mdr1b	5’-ATCTTCTGAGGTTCCGCTCA-3’	5’-ATACGCCAACAGCAGGTTTC-3’
Nanog	5’-CCAACCCAACTTGGAACAAC-3’	5’-GAAGTTATGGAGCGGAGCAG-3’
Nestin	5’-CTCGGGAGAGTCGCTTAGAG-3’	5’-ATTAGGCAAGGGGGAAGAGA-3’
Nkx2.5	5’-GGCTTTGTCCAGCTCCACT-3’	5’-CATTTTACCCGGGAGCCTAC-3’
Oct4	5’-TCTTCTGCTTCAGCAGCTTG-3’	5’-GTTGGAGAAGGTGGAACCAA-3’
Rat Anp	5’-GCCTTTTGGCTCCCAGGCCA-3’	5’-TCCAGGTGGTCTAGCAGGTTCTTG-3’
Rat Bnp	5’-GGCTGTGACGGGCTGAGGTTG-3’	5’-GGTGGTCCCAGAGCTGGGGAAAG-3’
Rat Gusb	5’-ACTCCTCACTGAACATGCGA-3’	5’-ATAAGATGTACCAGAAGCCA-3’
Rat α-Mhc	5’-GCGGACATTGCCGAGTCCCAG-3’	5’-TGGGATAGCAACAGCGAGGCTC-3’
Rat β-Mhc	5’-AGGGCGGACATTGCCGAGTC-3’	5’-CAGGCATCCTTAGGGTTGGGTAGC-3’
S100a4	5´- TTTGTGGAAGGTGGACACAA-3´	5´- CAGCACTTCCTCTCTCTTGG-3´
Sca-1	5’-GGCAGATGGGTAAGCAAAGA-3’	5’-CAATTACCTGCCCCTACCCT-3’

Primer	**Sense**	**Antisense**
Sdf1	5´-CAGCCGTGCAACAATCTGAAG-3´	5´-CTGCATCAGTGACGGTAAACC-3´
Sirt1	5´-GACACAGAGACGGCTGGAAC-3´	5´- CAGACCCTCAAGCCATGTTT-3´
Sm22	5'-GACTGCACTTCTCGGCTCAT-3'	5'-CCGAAGCTACTCTCCTTCCA-3'
Sox2	5'-AAAGCGTTAATTTGGATGGG-3'	5'-ACAAGAGAATTGGGAGGGGT-3'
Tbx5	5'-TGGTTGGAGGTGACTTTGTG-3'	5'-GGCAGTGATGACCTGGAGTT-3'
Tgfβ1	5'-CAACCCAGGTCCTTCCTAAA-3'	5'-GGAGAGCCCTGGATACCAAC-3'
Tie2	5'- TTTCGGCATCAGACACAAGA-3'	5'- CCGGCTTAGTTCTCTGTGGA-3'
Troponin T	5'-ACCCTCAGGCTCAGGTTCA-3'	5'-GTGTGCAGTCCCTGTTCAGA-3'
VE-Cadherin	5'-CGTTGGACTTGATCTTTCCC-3'	5'-CGCCAAAAGAGAGACTGGAT-3'
Vegfa	5'-AATGCTTTCTCCGCTCTGAA-3'	5'-GCTTCCTACAGCACAGCAGA-3'
vWF	5'-CTCACACAGAGCCACAAAGG-3'	5'-AACTGCGAGAGCTCTTCTGG-3'
α-Actinin	5'-TGTTCTCGATCTGTGTCCCC-3'	5'-CATGCAGCCTGAAGAGGACT-3'
α-Mhc	5'-CTTCATCCATGGCCAATTCT-3'	5'-GCGCATTGAGTTCAAGAAGA-3'
α-Sma	5'-GTTCAGTGGTGCCTCTGTCA-3'	5'-ACTGGGACGACATGGAAAAG-3'
β-Mhc	5'-GAGCCTTGGATTCTCAAACG-3'	5'-GTGGCTCCGAGAAAGGAAG-3'

Table S3. Echocardiographic data in the rat MI model. Related to Fig 2.

	Vehicle (n=5)	Control-miR–CPCs (n=6)	miR-133a–CPCs (n=11)
Baseline (before MI)			
LVEDD (mm)	5.12 ± 0.13	5.63 ± 0.19	5.13 ± 0.25
LVESD (mm)	3.16 ± 0.16	3.60 ± 0.21	2.81 ± 0.27
LVAd (mm^2)	29.87 ± 0.98	24.16 ± 1.47	22.21 ± 1.35
LVAs (mm^2)	8.60 ± 0.33	7.11 ± 0.56	6.04 ± 0.43
AWdT (mm)	1.79 ± 0.04	1.13 ± 0.04	1.64 ± 0.09
AWsT (mm)	2.78 ± 0.04	1.92 ± 0.19	2.51 ± 0.13
FS (%)	38.24 ± 0.84	36.25 ± 1.81	46.17 ± 3.44
FAC (%)	71.16 ± 0.39	70.48 ± 1.63	72.22 ± 1.94
AWTF (%)	35.58 ± 1.18	39.19 ± 4.75	34.76 ± 1.26
2 weeks (after treatment)			
LVEDD (mm)	7.17 ± 0.34	6.33 ± 0.52	6.57 ± 0.21
LVESD (mm)	5.64 ± 0.36	4.20 ± 0.36	4.15 ± 0.26
LVAd (mm^2)	43.80 ± 1.86	37.06 ± 2.75	33.39 ± 1.42
LVAs (mm^2)	28.36 ± 1.39	16.73 ± 2.88	13.24 ± 0.92
AWdT (mm)	1.29 ± 0.20	1.66 ± 0.15	1.66 ± 0.06
AWsT (mm)	1.64 ± 0.26	2.40 ± 0.12	2.43 ± 0.15
FS (%)	21.62 ± 1.83	33.65 ± 1.23[a]	37.24 ± 2.48[a]
FAC (%)	35.15 ± 1.05	56.23 ± 5.11[a]	60.63 ± 1.80[a]
AWTF (%)	21.19 ± 1.07	31.68 ± 3.30[a]	31.52 ± 1.52[a]
4 weeks (after treatment)			
LVEDD (mm)	7.65 ± 0.23	6.67 ± 0.39	7.06 ± 0.24
LVESD (mm)	6.11 ± 0.25	4.72 ± 0.54	4.66 ± 0.33
LVAd (mm^2)	50.89 ± 4.96	46.15 ± 4.35	41.34 ± 2.13
LVAs (mm^2)	39.35 ± 4.44	27.33 ± 4.40	17.23 ± 1.75
AWdT (mm)	1.42 ± 0.40	1.54 ± 0.19	1.71 ± 0.08
AWsT (mm)	1.67 ± 0.41	2.08 ± 0.20	2.47 ± 0.15
FS (%)	20.28 ± 1.32	30.19 ± 4.52	34.72 ± 2.68[a]
FAC (%)	23.15 ± 0.61	42.37 ± 6.42[a]	59.08 ± 2.51[ab]
AWTF (%)	16.71 ± 2.06	25.12 ± 5.92	29.97 ± 2.41[a]

LVEDD: left ventricular end-diastolic diameter. LVESD: left ventricular end-systolic diameter. LVAd: left ventricular area at diastole. LVAs: left ventricular area at systole. AWdT: anterior wall diastolic thickness. AWsT: anterior wall systolic thickness. FS: fractional shortening, calculated as FS (%) = [(LVEDD - LVESD)/LVEDD] x 100. FAC: fractional area change, calculated as FAC (%) = [(LVAd - LVAs)/LVAd] x 100. AWTF: anterior wall thickening fraction, calculated as AWTF (%) = [(AWdT - AWsT)/ AWdT] x 100. [a,] $P<0.05$ versus vehicle. [b,] $P<0.05$ versus control-miR-CPCs.

Table S4. Morphometric data in the rat MI model. Related to Fig 3.

	Vehicle (n=5)	**Control-miR-CPCs (n=7)**	**miR-133a-CPCs (n=7)**
LV area (mm^2)	23.39 ± 4.59	21.33 ± 2.81	25.92 ± 2.44
LV cavity (mm^2)	20.02 ± 4.77	7.73 ± 2.14	5.30 ± 1.66
Risk region area (mm^2)	12.61 ± 2.80	8.36 ± 0.74	8.34 ± 0.85
Scar region area (mm^2)	10.45 ± 1.83	6.74 ± 0.86	4.65 ± 0.96
Infarcted wall thickness (mm)	0.60 ± 0.15	0.46 ± 0.02	0.80 ± 0.05
Risk area (% of LV)	53.42 ± 3.25	41.82 ± 4.30	31.77 ± 4.10[a]
Scar area (% of risk region)	45.55 ± 3.48	33.32 ± 3.71[a]	17.28 ± 4.03[a,b]
Viable myocardium (% of risk region)	14.85 ± 4.04	20.90 ± 4.40	48.26 ± 8.81[a,b]

LV, left ventricle. [a] P <0.05 versus vehicle; [b] P <0.05 versus control-miR-CPCs.

SUPPLEMENTAL EXPERIMENTAL PROCEDURES

Animals

Cardiac progenitor cells (CPCs) were isolated from adult female C57BL/6 mice. Neonatal rat cardiomyocytes (NRCMs) were isolated from newborn Wistar rats. Myocardial infarction was conducted in adult male Wistar rats or adult female C57BL/6 mice. The corresponding local ethics committee approved animal studies. All animal procedures conformed to EU Directive 86/609/EEC and Recommendation 2007/526/EC regarding the protection of animals used for experimental and other scientific purposes, enforced in Spanish law under Real Decreto 1201/2005.

Isolation, culture and surface marker characterization of Sca-1$^+$ CPCs

C57BL/6 mice between 8 and 12 weeks of age were anesthetized with ketamine (100 mg/kg)/xylacine (10 mg/kg). After cannulation of the aorta, the heart was removed and perfused *ex vivo* through the coronary system during 10-20 minutes with a solution of 4mg/mL collagenase type II (Worthington). The digested hearts were minced and mechanically disaggregated, and the resulting cell suspension was passed through a 70μm filter. The fraction of small live cells was obtained by density gradient centrifugation with OptiPrep^{TM} (Axis-Shield), and the SCA-1$^+$ hematopoietic lineage negative fraction was purified by magnetic cell sorting using a lineage cell depletion kit and Sca-1 microbeads (Miltenyi Biotec). The isolated cells were cultured in DMEM/F12 (Invitrogen) supplemented with 10% ES-qualified FBS (Invitrogen), 20 ng/mL bFGF (Peprotech), 40 ng/mL EGF (Sigma), 10^3 U/mL LIF (Millipore), 1% insulin-transferrin-selenium (Invitrogen), 1% penicillin/streptomycin (Lonza) and 1% L-glutamine (Lonza). Cell surface markers were analyzed by flow cytometry in a BD

FACSCanto II flow cytometer using BD FACSDiva software (Becton Dickinson). SCA-1^+ CPCs were stained with antibodies in ice-cold PBS, 0.5% BSA, 2 mM EDTA.

Myocardial infarction and cell injection

Myocardial infarction models were as described previously, with small variations (Arminan et al., 2010, Fischer et al., 2009)**.** Briefly, male Wistar rats (6 weeks old) or female C57BL/6 mice (12 weeks old) underwent left thoracotomy under general anesthesia with 2.5% sevofluorane, and were ventilated with a rodent respirator. In the rat model animals were treated with 20 mg/kg/day of cyclosporine A (Novartis) for 3 days before the procedure until sacrifice. Myocardial infarction was induced by permanent ligation of the left anterior descending coronary artery. At five minutes post ligation, 10^5 CPCs (control-miR–CPCs or miR-133a–CPCs suspended in 21µl PBS as vehicle) or vehicle were injected by a blinded surgeon into three sites around infarct border zone. In the rat model, the cell suspension contained red fluorescent microbeads ($6.25x10^6$ beads/animal; Molecular Probes). Animals that underwent thoracotomy without artery ligation or cell injection were used as sham controls. After injections, the chest was closed and animals allowed recovering.

Cardiac function was monitored by echocardiography 1 day before the ligation (baseline) and 2 and 4 weeks after surgery, using the Vivid 7 echocardiography system (GE Healthcare, Little Chalfont, UK). Vivid S5 10.1.x software (GE Healthcare) was used to measure fractional area change (FAC) from the 2D-Mode of the short-axis view and fractional shortening (FS) from the M-mode of the short axis view.

Neonatal rat cardiomyocyte *in vitro* assays

Neonatal rat cardiomyocytes (NRCMs) were obtained from 0-2 day old Wistar rats. Hearts were minced and cells separated by digestion with trypsin (Invitrogen, NY, USA) and collagenase type II (Worthington) followed by differential plating. After 2 days, seeding onto a NRCM monolayer, followed by co-culture for 7 days, induced CPC differentiation. Apoptosis in serum starved NRCMs was monitored by TUNEL staining (Cell Death Detection Kit; Roche, Basel, Switzerland) of troponin-positive cells. NRCM apoptosis (caspase-3/9) and hypertrophy (cardiomyocyte area; ImageJ, NIH) were also measured in response to H_2O_2 (50 µmol/L, 2 hours) or angiotensin II (ANGII, 100 nmol/L, 72 hours; Sigma) in the presence of CPC conditioned medium (CM).

Differentiation of CPCs toward the cardiac, smooth muscle and endothelial lineages

Cardiac differentiation

Differentiation was promoted by seeding CPCs at $2x10^4$ cells/cm^2 in culture medium, and replacing medium after 24 hours with α-MEM supplemented with 10% FBS, 1% penicillin/streptomycin, 1% L-glutamine and 10nM dexamethasone. At 0, 3, 7, 10 and 14 days, samples were collected for gene expression and western-blot analysis.

For co-culture differentiation experiments, NRCMs were seeded at $7.5x10^4$ cells/cm^2 on gelatin-coated plates or slides. Medium was changed the next day, and after 72 hours, GFP^+ CPCs were seeded onto the NRMC monolayer at $3x10^3$ /cm^2 in cardiomyocyte medium without cytosine β-D-arabinofuranoside. Co-culture was continued for 7 to 10

days. For immunofluorescence analysis cells were fixed in 4% PFA. For gene expression and western blot analysis cells were collected by trypsinization, and CPC-derived (GFP^+) cells were isolated by cell sorting with a FACSAria SORP (Becton Dickinson).

Smooth muscle differentiation

For smooth muscle differentiation CPCs were seeded at $2x10^4$ cells/cm^2 in culture medium, and after 24 hours medium was replaced with medium supplemented with 100nM oxytocin. After 3 days, medium was changed to DMEM/F12 supplemented with 10% FBS, 1% penicillin/streptomycin, 1% L-glutamine, 10mM β-glycerophosphate, 1 μM dexamethasone and 0.2 mM ascorbic acid. After 7 days cells were fixed in 4% PFA and analyzed by immunofluorescence.

Endothelial differentiation

For endothelial differentiation *in vitro*, CPCs were seeded at $2x10^4$ cells/cm^2 in culture medium, and after 24 hours medium was replaced with DMEM/F12 supplemented with 2% FBS, 1% penicillin/streptomycin, 1% L-glutamine, 50 ng/mL VEGF, 20 ng/mL IGF-1, 10 ng/mL EGF, 50 ng/mL ECGF and 1 μg/mL hydrocortisone. Cells were collected 4 days later for gene expression analysis.

Endothelial differentiation *in vivo* was evaluated by Matrigel angiogenesis plug assay. Matrigel mixed with 10^5 GFP^+ CPCs was injected subcutaneously into the backs of 12 week-old C57BL/6 female mice. After 7 days the animals were sacrificed and the implants formed were fixed and paraffin embedded, and 5μm sections were analyzed by immunofluorescence.

CPC proliferation

MTT metabolic assay. Control-miR–CPCs, miR-1–CPCs and miR-133a–CPCs were seeded at $5x10^3$ cell/cm^2 in 24 well plates, and the MTT assay was performed at 24, 48, 72 and 96 hours after plating in 3 independent wells per condition, using the Cell Proliferation Kit I (MTT) from Roche.

^{3}H-thymidine incorporation. Control-miR–CPCs, miR-1–CPCs and miR-133a–CPCs were seeded at $5x10^3$ cell/cm^2 in 24 well plates, and the next day medium was switched to DMEM/F12 supplemented with 1% penicillin/streptomycin and 1% L-glutamine. Twenty-four hours later, medium was replaced with fresh medium supplemented with 1 µCi/mL [6-^{3}H]-thymidine (Perkin-Elmer). After 48 hours, cells were fixed and collected, and ^{3}H-thymidine incorporation was measured by standard scintillation counting.

CPC apoptosis

Before H_2O_2 treatment, CPCs were incubated overnight with serum-free DMEM/F12. The next day, cells were treated with 200 µmol/L H_2O_2 for 0, 2 or 5 hours, and samples were collected for gene expression analysis, protein lysate isolation or apoptosis quantification. The percentage of living cells was measured by FACS after staining with annexin V-FITC and propidium iodide (PI) (0.01%), with an apoptosis detection kit (BD Pharmingen). Caspase-3 activity was measured by fluorescence intensity with the CaspGLOW Green caspase-3 staining (MBL International). Cytochrome c release was measured with the Rat/Mouse Cytochrome c Quantikine ELISA Kit (R&D Systems).

Osteogenic and adipogenic differentiation of CPCs

CPCs were seeded at $2x10^4$ cells/cm^2 in culture medium, and after 24 hours, medium was replaced by the corresponding induction medium. Osteogenic medium was α-MEM

supplemented with 10% FBS, 1% penicillin/streptomycin, 1% L-glutamine, 10 mM β-glycerophosphate, 0.1 μM dexamethasone and 0.2 mM ascorbic acid. Adipogenic medium was α-MEM supplemented with 10% FBS, 1% penicillin/streptomycin, 1% L-glutamine, 0.5 μM hydrocortisone, 0.5 mM IBMX (3-isobutyl-1-methyl xanthine) and 60μM indomethacin; in all cases, induction medium was replaced every 3–4 days, and on day 21 cells were processed for histochemical analysis. Cells were fixed in 70% ethanol (1 hour, 4°C) and stained (5 minutes). For osteogenic assays, cells were stained with 40 mM Alizarin Red, pH 4.1. Cells cultured in adipogenic medium were stained with 2% Oil Red O.

Conditioned media

Control-miR–CPCs and miR-133a–CPCs were seeded at 80% confluence, and after 24 hours cells were washed with PBS and culture medium was replaced with M199 Glutamax supplemented with 10mM HEPES, 0.1mM MEM non essential amino acids and 1% penicillin/streptomycin (apoptosis and hypertrophy experiments). After 48 hours, conditioned medium was collected, centrifuged to eliminate cell debris, and stored at -80°C until use. The exosomal fraction was isolated by differential ultracentrifugation as described previously (Thery et al., 2006). Briefly, cleared conditioned medium was centrifuged for 10 minutes at 2,000g, the supernatant was collected and centrifuged for 30 minutes at 10,000g, and the supernatant was again collected and centrifuged at 100,000g for 70 minutes to pellet the exosomes, which were recovered and washed to eliminate contaminating proteins.

Synthetic miRNA transfection and Bim 3'UTR luciferase reporter assay

To confirm *Bim* as a target of miR-133a, a 1 kb fragment of the mouse *Bim* 3'UTR containing the putative binding site for miR-133a at nucleotides 1545-1551 was amplified by PCR from C57BL/6 mouse genomic DNA using the primers FW: 5'-

CTCGAGTGGGCTCACACACCGCTTGC-3' and RV: 5'-GCGGCCGCACAGGGCC TCATGGGAACCA-3'. To confirm *Bmf* as a target of miR-133a a 1 kb fragment of the mouse *Bmf* 3'UTR containing the putative binding site for miR-133a at nucleotides 2153-2160 was amplified as described above using the primers FW: 5'-CTCGAGTGCAAGGAGAGGGGACCCAAG-3' and RV: 5'-GCGGCCGCAGTAGA GCAGTTTGGCCCCTGA-3'. Fragments were subsequently cloned into a psiCHECK-2 vector (Promega) downstream of the *Renilla* luciferase reporter gene.

For luminescence assays, 293T cells were seeded at 10^5 cell/cm^2 in 24 well plates, and transfected 24 hours later using Lipofectamine 2000 (Invitrogen) with 250 ng of the reporter vector and 30 nM of the different LNA's: a scramble miRNA, a synthetic miR-133a or a miR-133a inhibitor (antimiR, all from Ambion). The ratio of *Renilla* to firefly luciferase luminescence was measured 24 hours later with the Dual luciferase assay system (Promega). Normalized *Renilla* to firefly ratios were determined in absence, presence or inhibition of miR-133a.

Bioinformatic analysis of predicted targets for miR-133a

Analysis and selection of targets predicted to be affected by miR-133 was developed by means of Ingenuity Analysis Pathway Software (IPA), which identifies mRNA targets for microRNAs using predicted microRNA–mRNA binding relationships from TargetScan, plus experimentally validated relationships from TarBase and curated by direct research from the biomedical literature. We first generated an initial dataset of predicted targets for miR-133a based on the results of 10 different algorithms (DIANAmT, miRanda, miRDB, miRWalk, PICTAR4, PICTAR5, PITA, RNA22, RNAhybrid and TargetScan). We accurated this list by selecting common targets predicted by at least 5 algorithms and this second dataset was analysed by Ingenuity

Pathway Analysis (IPA) software. The final selection of targets to test was complemented with a detailed review of the literature.

Protein lysates and Western blotting

Cells were lysed in RIPA buffer containing protease inhibitors (Roche) and, after centrifugation, supernatants were collected and protein quantified by the DC protein assay (Biorad). Protein (30µg per lane) was loaded on 4-12% gels (Biorad) and Western blotting was performed in the mini protean III system (Biorad). Membranes were blocked and incubated overnight with primary antibodies against α-actinin (1:500, Sigma) and troponin T (1:1000, Abcam), diluted in 5% non-fat milk in PBS, 0.1% Tween 20 (Sigma). Next day, membranes were incubated with the corresponding horseradish peroxidase (HRP)-conjugated secondary antibodies (Dako), and blots were developed with the ECL kit (GE Healthcare).

FACS analysis

Cells were stained with antibodies against NKX2.5 (1:50, Santa Cruz Biotech), α-actinin (1:100, Sigma), troponin I (1:100, Santa Cruz Biotech) or tropomyosin (1:100, Sigma), in ice-cold PBS, 0.5% BSA, 2 mM EDTA for 30 minutes (Table S1). Cells were then incubated with Cy3/FITC/PE-conjugated secondary antibodies (Jackson Immunoresearch). Secondary antibodies alone (goat anti-rabbit IgG or anti-mouse IgG, Cy3 conjugated) or combined with irrelevant primary antibodies were used as negative controls for gating purposes. Staining was analyzed by flow cytometry in a BD FACSCanto II flow cytometer using BD FACSDiva software (Becton Dickinson). In some cases staining was visualized by microscopy after cell cytospin.

Immunocytochemistry

Coverslips or chamber slides (Nunc) from differentiation or apoptosis experiments were washed with PBS, and the cells were fixed in 4% paraformaldehyde (PFA) at room temperature, permeabilized with 0.1% Triton-X, blocked with 10% goat serum and incubated overnight at 4ºC with primary antibodies in 1% goat serum. Primary antibodies used are listed in supplementary table 1 (Table S1). The next day, cells were washed and incubated for 45 minutes at room temperature with secondary antibody conjugated with Alexa Fluor 488 or Alexa Fluor 649 (Invitrogen) or with Cy3 (Jackson Immunoresearch). Incubation with secondary antibody alone did not produce any detectable background signal. Slides were mounted in Vectashield with Dapi (Vector labs) and analyzed by confocal microscopy (Leica SP5, Leica).

RNA Isolation, RT-PCR and real time RT-PCR

Total RNA was isolated with the miRNeasy Mini Kit (Qiagen). For protein-coding genes, cDNA was obtained with Superscript III Reverse Transcriptase (Invitrogen), and sequences were amplified by PCR using the primers listed in Table S2; *Gapdh* or *Gusb* were used as endogenous normalization controls. PCR amplification and Quantitative PCR were performed with Taq DNA Polymerase (Roche) and Power SYBR-Green Master Mix (Applied Biosystems), respectively. miR-1 and miR-133a transcripts were quantified by real-time RT-PCR using the corresponding TaqMan Gene Expression Assays (Applied Biosystems), and U6 was used as an endogenous normalization control. PCR products were quantified with an ABI PRISM 7900 quantitative PCR system (Applied Biosystems) and analyzed with SDS v2.3 software (Applied Biosystems).

Echocardiography

Transthoracic echocardiograms were obtained by a blinded echocardiographer to assess cardiac function. In the rat model echocardiography was performed 1 day before the ligation (baseline) and at 2 and 4 weeks after surgery, under general anesthesia (2.5% sevofluorane), using an echocardiographic system (Vivid 7; GE Healthcare) equipped with a 10-MHz linear-array transducer. In the mouse model, echocardiography was performed 1 week and 12 weeks after surgery, under general anesthesia (2.5% sevofluorane), using the Vevo 770 Imaging System (VisualSonics). The hearts were imaged two-dimensionally in long-axis view (at the level of the greatest LV diameter) and in the short-axis view (at the level of the papillary muscle). In the rat model, fractional area change (FAC) was calculated from the 2D-mode of the short axis view while fractional shortening (FS) was calculated from the M-mode of the short axis view with Vivid S5 10.1.x (GE Healthcare). In the mouse model fractional area change (FAC) and left ventricular ejection fraction (LVEF) were calculated from the long-axis view with VisualSonics V1.3.8 (VisualSonics). Measurements of cardiac parameters and formulas for calculations are described in supplementary table 3. Animals with extremely small infarcts or showing poor echocardiography images were excluded.

Morphology and histology

Rats were sacrificed 4 weeks after MI and the hearts fixed for histology. Eight sections per heart, covering the organ from apex to base, were stained with Masson's trichrome. Computer planimetry analysis of the Masson's trichromic images (Image Pro-Plus 5.1, Media Cybernetics, MD, USA) was used to calculate left ventricle (LV) morphometric parameters (LV cavity area, LV total area, risk region area, scar area and LV anterior wall thickness) for each section.

GFP^+ cells in the myocardium were detected by immunohistochemistry with an anti-GFP antibody (Abcam, Cambridge, United Kingdom). α-SMA^+ blood vessels were quantified by α-SMA staining (anti-α-SMA; Sigma, MO, USA) and cardiomyocyte cross-sectional area was measured by analysis of Laminin staining (anti-Laminin; Abcam) with ImageJ (NIH). To study cardiomyocyte proliferation, rats were injected with EdU (5-ethynyl-2´-deoxyuridine; 10 mg/kg/day) for 5 days prior to sacrifice. The EdU signal was detected in 3 sections per heart using the Click-iT EdU Alexa Fluor 647 Imaging Kit (Molecular Probes, NY, USA), and sections were stained with anti-troponin T antibody. The number of total EdU^+ cells and EdU^+ cardiomyocytes in the border zone was measured with ImageJ (NIH).

Immunohistochemistry

Rat heart cryosections were washed with PBS at room temperature and permeabilized with 0.1% Triton-X. Mouse heart paraffin-embedded sections were deparaffinized, rehydrated, washed with PBS, and antigens were retrieved with sodium citrate. For tyramide amplification, slides were incubated with 0.3% H_2O_2. Tissue sections were then blocked with 10% goat serum or Perkin-Elmer blocking buffer (in the case of tyramide amplification) and incubated overnight at 4ºC in blocking solution with primary antibodies. All primary antibodies used are specified in Table S1. Slides were washed and incubated for 1 hour at room temperature with secondary antibodies conjugated to Alexa Fluor 488 or Alexa Fluor 649 (Invitrogen), to Cy3 (Jackson Immunoresearch), or to HRP (Dako). Incubation with secondary antibody alone did not give any detectable background signal. Slides were mounted in Vectashield with DAPI (Vector labs) and analyzed by confocal microscopy (Leica SP5, Leica).

Detection of GFP^+cells. CPCs (or their progeny) were detected in heart sections either by direct visualization of GFP protein fluorescence or by immunostaining with an ant-

GFP antibody; the anti-GFP antibody signal was amplified with tyramide (TSA, Perkin-Elmer). To evaluate the cardiac fate of transplanted CPCs and derived GFP^+ cells, sections were also incubated with an anti-Troponin T or anti-Tropomyosin antibody.

α-Sma$^+$ blood vessel quantification. To study arteriolar density in the rat model, 3 sections from each heart were stained with antibodies against troponin T and α-SMA, and the number of α-SMA^+ blood vessels/mm^2 was quantified in 4 image fields per section of the remote (healthy) myocardium and 6 image fields per section in the border zone.

Cardiomyocyte proliferation. Rats were injected daily with EdU (10 mg/kg/day) for 5 days prior to sacrifice. EdU signal was detected in 3 sections per heart using the Click-iT EdU Alexa Fluor 647 imaging kit (Molecular Probes), and sections were stained with troponin T antibody. The number of EdU^+ total cells and EdU^+ cardiomyocytes in the border zone was quantified in 10 image fields per section using ImageJ (NIH).

In vivo cardiomyocyte hypertrophy. To analyze cardiomyocyte hypertrophy in the border zone of the infarct, two sections from each rat heart were stained with antibodies against Troponin T and Laminin, and cross-sectional area of cardiomyocytes was calculated in 4 image fields per slide using ImageJ (NIH).

NRCM *in vitro* hypertrophy assay

NRCMs were seeded at $1.2x10^5$ cells/cm^2 on gelatin-coated slides, and the next day medium was switched to medium without FBS. After overnight incubation, cells were cultured in CPC-conditioned medium supplemented with 100 nM ANG II for 72 hours. Cells were fixed in 4% PFA and stained with troponin T primary antibody, and cell area was measured in 3 image fields per slide in 3 independent slides with NIH ImageJ software.

NRCM apoptosis assays

Co-culture with CPCs and serum starvation

NRCMs were seeded at 10^4 cells/cm^2 on gelatin-coated slides. The medium was changed the next day, and after 24 hours $6x10^4$ CPCs/cm^2 were seeded onto the monolayer in cardiomyocyte medium free of FBS or horse serum. Co-culture was continued for 3 or 7 days, when cells were fixed with 4% PFA and stained with anti-troponin T (Abcam). Apoptotic cardiomyocytes were quantified by TUNEL staining of troponin T^+ cells in 10 image fields per slide on 3 independent slides using the fluorescein cell death detection kit, (Roche).

Apoptosis experiments with H_2O_2

NRCMs were seeded at $3x10^5$ cells/cm^2 on gelatin-coated 96 well optical plates. The medium was changed the next day with medium containing 2% FBS, and after 48 hours cells were incubated overnight with conditioned medium from CPCs. The next day, 50 mM H_2O_2 was added and, after 2 hours Caspase 3 and Caspase 9 activities were measured by fluorescence intensity with the CaspGLOW Green caspase-3 staining and CaspGLOW Green caspase-9 staining kits (MBL International).

Engineered Heart Muscle (EHM) assays

EHM generation

Engineered Heart Muscle (EHM) was generated as described (Zimmermann et al., 2000; Zimmermann et al., 2002). Neonatal rat heart cells were prepared by Trypsin/DNAse digestion. For the construction of CPC-EHMs, rat heart cells were preplated for 60 min in DMEM (Biochrom), 10% FBS, 2 mmol/L Glutamine, 100 U/ml penicillin, and 100 µg/ml streptomycin (all from Invitrogen), to enrich for

cardiomyocytes (Fig 7). Enriched cardiomyocytes were then mixed with CPCs (3:1) in a hydrogel containing 0.8 mg pH-neutralized rat-tail collagen, 10% v/v basement membrane protein from Engelbreth-Holm-Swarm tumor exudates (BD Biosciences), and concentrated culture medium (2xDMEM, 20% horse serum, 4% chick embryo extract, 200 U/ml penicillin, and 200 µg/ml streptomycin, all from Invitrogen). Subsequently, the EHM-mixture was cast into custom made-molds. EHM culture medium consisted of DMEM (Biochrom), 10% horse serum, 2% chick embryo extract, 100 U/ml penicillin, and 100µg/ml streptomycin. EHMs were transferred to stretch devices on culture day 7 for continuous culture under phasic load (from 100 to 110% of slack length at 2 Hz) for additional 5 days.

Isometric Force Measurements

On day 12, EHMs were transferred to organ baths containing oxygenated Tyrode's solution at 37°C. EHMs were preloaded under electrical stimulation (200 mA, 5 ms, 2 Hz). Twitch tension was measured under increasing calcium concentrations (0.2–2.8 mmol/L). Contractile activity and twitch parameters were evaluated using AMON software.

Flow cytometry

Neonatal rat heart cells, before and after preplating, were fixed in ice-cold 70% ethanol. Staining for α-Actinin (Sigma) was performed in the presence of 0.5% Triton-X at 4°C for 45 min. Alexa 546-coupled anti-mouse secondary antibody was applied for 30 min at 4°C. Samples were run on a LSRII SORP cytometer (BD Biosciences) and analyzed with Cyflogic software.

EHM histology

EHMs were fixed in neutral buffered 4% formaldehyde/1% methanol, pH 7.4 overnight, followed by extensive washing with PBS. For whole mount staining, EHMs were incubated in blocking buffer (PBS, 0.5% Triton-X, 5% goat serum, 1% BSA) overnight, followed by 2 nights incubation with primary antibodies. Primary antibodies applied were against α-actinin (1:1000; Sigma), active caspase-3 (1:250; Promega) and GFP (1:500; abcam). After extensive washing, appropriate secondary antibodies and DAPI (1 µg/ml) were incubated overnight followed by extensive washing.

EHM sections were imaged with a Zeiss LSM 710 confocal microscope. For cell quantification, at least 8 random sections per EHM were imaged and analyzed by an independent observer using ImageJ software.

SUPPLEMENTAL REFERENCES

Arminan, A., Gandia, C., Garcia-Verdugo, J. M., Lledo, E., Trigueros, C., Ruiz-Sauri, A., Minana, M. D., Solves, P., Paya, R., Montero, J. A., et al. (2010). Mesenchymal stem cells provide better results than hematopoietic precursors for the treatment of myocardial infarction. J Am Coll Cardiol. *55*, 2244-2253.

Fischer, K. M., Cottage, C. T., Wu, W., Din, S., Gude, N. A., Avitabile, D., Quijada, P., Collins, B. L., Fransioli, J. and Sussman, M. A. (2009). Enhancement of myocardial regeneration through genetic engineering of cardiac progenitor cells expressing Pim-1 kinase. Circulation. *120*, 2077-2087.

Thery, C., Amigorena, S., Raposo, G. and Clayton, A. (2006). Isolation and characterization of exosomes from cell culture supernatants and biological fluids. Curr Protoc Cell Biol. *Chapter 3*, Unit 3 22.

Zimmermann, W. H., Fink, C., Kralisch, D., Remmers, U., Weil, J. and Eschenhagen, T. (2000). Three-dimensional engineered heart tissue from neonatal rat cardiac myocytes. Biotechnol Bioeng. *68*, 106-114.

Zimmermann, W. H., Schneiderbanger, K., Schubert, P., Didie, M., Munzel, F., Heubach, J. F., Kostin, S., Neuhuber, W. L. and Eschenhagen, T. (2002). Tissue engineering of a differentiated cardiac muscle construct. Circ Res. *90*, 223-230.